

Mutation of the Membrane-Associated M1 Protease APM1 Results in Distinct Embryonic and Seedling Developmental Defects in *Arabidopsis*

Wendy Ann Peer,^{a,1} Fazeeda N. Hosein,^{a,1} Anindita Bandyopadhyay,^{a,1,2} Srinivas N. Makam,^{a,3} Marisa S. Otegui,^b Gil-Je Lee,^a Joshua J. Blakeslee,^{a,4} Yan Cheng,^a Boosaree Titapiwatanakun,^a Bahktiyor Yakubov,^a Bharat Bangari,^a and Angus S. Murphy^{a,5}

^aDepartment of Horticulture, Purdue University, West Lafayette, Indiana 47907

^bDepartment of Botany, University of Wisconsin, Madison, Wisconsin 53706

Amino peptidase M1 (APM1), a single copy gene in *Arabidopsis thaliana*, encodes a metallopeptidase originally identified via its affinity for, and hydrolysis of, the auxin transport inhibitor 1-naphthylphthalamic acid (NPA). Mutations in this gene result in haploinsufficiency. Loss-of-function mutants show irregular, uncoordinated cell divisions throughout embryogenesis, affecting the shape and number of cotyledons and the hypophysis, and is seedling lethal at 5 d after germination due to root growth arrest. Quiescent center and cell cycle markers show no signals in *apm1-1* knockdown mutants, and the ground tissue specifiers *SHORTROOT* and *SCARECROW* are misexpressed or mislocalized. *apm1* mutants have multiple, fused cotyledons and hypocotyls with enlarged epidermal cells with cell adhesion defects. *apm1* alleles show defects in gravitropism and auxin transport. Gravitropism decreases *APM1* expression in auxin-accumulating root epidermal cells, and auxin treatment increases expression in the stele. On sucrose gradients, *APM1* occurs in unique light membrane fractions. *APM1* localizes at the margins of Golgi cisternae, plasma membrane, select multivesicular bodies, tonoplast, dense intravacuolar bodies, and maturing metaxylem cells. *APM1* associates with brefeldin A-sensitive endomembrane structures and the plasma membrane in cortical and epidermal cells. The auxin-related phenotypes and mislocalization of auxin efflux proteins in *apm1* are consistent with biochemical interactions between *APM1* and NPA.

INTRODUCTION

APM1, an M1 aminopeptidase (AtM1.10.1, MEROPS peptidase classification) and founding member of the M1 family of metallopeptidases in *Arabidopsis thaliana*, was originally identified by its affinity for and hydrolysis of the noncompetitive auxin efflux inhibitor 1-naphthylphthalamic acid (NPA) (Murphy and Taiz, 1999a, 1999b; Murphy et al., 2000, 2002). APM1 exhibits aminopeptidase (AP) activity against N-terminal neutral/aromatic-hydroxyl amino acids of peptides but also functions as an amidase that slowly cleaves the amide bond of NPA (Murphy and Taiz, 1999a, 1999b; Murphy et al., 2000, 2002). This property

made it possible to purify APM1 by NPA affinity chromatography from *Arabidopsis* microsomal and plasma membrane fractions (Murphy et al., 2002). Hydrolysis by APM1 appears to require immobilization of NPA by a complex that includes the peripheral immunophilin-like protein FKBP42/TWD1, and the integral membrane auxin transport proteins ABCB1/PGP1 and ABCB19/PGP19/MDR1 (Murphy et al., 2000, 2002; Noh et al., 2001; Geisler et al., 2003; Petrásek et al., 2003; Bouchard et al., 2006; Blakeslee et al., 2007; Bailly et al., 2008). A role for APM1 in subcellular protein trafficking was suggested by its copurification with β -adaptin subunits of the adaptor trafficking complexes, the dynamin ADL1a/DRP1a, the HSC70 homolog HSP70p, and an ortholog of the SEC14 lipid transfer protein (Murphy et al., 2002).

NPA has been shown to partially inhibit auxin efflux mediated by PINFORMED (PIN) and ABCB/PGP transporters and to completely inhibit auxin export when the two types of exporters are coexpressed in heterologous systems (Petrásek et al., 2003, 2006; Geisler et al., 2005; Blakeslee et al., 2007; Rojas-Pierce et al., 2007). NPA (1 to 5 μ M) inhibits the basal polar auxin flow required for establishment of embryonic apical/basal polarity and organogenesis (Weijers et al., 2005; Mravec et al., 2008). Higher concentrations (≥ 50 μ M) of NPA inhibit trafficking and produce phenotypes observed in PIN1 and other general trafficking components (Gil et al., 2001; Geldner et al., 2001, 2004; Peer et al., 2004; Růzicka et al., 2007), inducing embryonic defects in *Arabidopsis* and other species (reviewed in Friml, 2003; Friml et al., 2003; Weijers et al., 2005; Larsson et al., 2008;

¹ These authors contributed equally to this work.

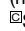
² Current address: Department of Biology, Washington University, St. Louis, MO 63108.

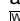
³ Current address: Department of Biology, Arizona State University, Tempe, AZ 85287.

⁴ Current address: Department of Molecular Biology, Cell Biology, and Biochemistry, Brown University, Providence, RI 02912.

⁵ Address correspondence to murphy@purdue.edu.

The authors responsible for distribution of materials integral to the findings presented in this article in accordance with the policy described in the Instructions for Authors (www.plantcell.org) is: Angus S. Murphy (murphy@purdue.edu).

 Some figures in this article are displayed in color online but in black and white in the print edition.

 Online version contains Web-only data.

www.plantcell.org/cgi/doi/10.1105/tpc.108.059634

Hakman et al., 2009), similar to those observed with brefeldin A (BFA) treatment (Friml et al., 2003). This suggests that NPA at $>5 \mu\text{M}$ has nonspecific targets, especially as very high concentrations approach NPA solubility limits $\sim 280 \mu\text{M}$. Results presented by Murphy and Taiz (1999a) suggest that APM1 is a target of the 3 to 50 μM range. NPA effects in these concentrations are mimicked by AP inhibition by aminoacyl naphthylamide conjugates resembling NPA and produce additional phenotypes not associated with auxin defects.

The pharmacological treatment with NPA phenocopies loss-of-function lesions in *GNOM* (*GN*), *MONOPTEROS* (*MP*) (Mayer et al., 1991, 1993), *BODENLOS* (*BDL*) (Hamann et al., 2002), quadruple *PIN* (Friml et al., 2003), and *APM1* (presented here). This suggests that high concentrations of NPA affect more than just auxin transport and are indeed altering protein targeting or trafficking. Therefore, there are distinct classes of NPA effects based on the concentration used. Lower NPA concentrations inhibit auxin efflux without affecting the subcellular localization of the transport proteins, while high NPA concentrations alter the subcellular localization of the transporters and also induced embryonic and seedling defects.

We have also shown that APM1 enzymatic activity is sensitive to NPA (Murphy et al., 2002). NPA inhibition of APM1 activity occurs in the mid-to-high concentration range corresponding to non-auxin-related phenotypes, inhibition of trafficking, and defects in embryogenesis (Murphy and Taiz, 1999a; Murphy et al., 2002). APM1 activity is also sensitive to PAQ22, a phthalimide inhibitor of mammalian microsomal APs that is structurally similar to NPA, as well as puromycin, bestatin, and amastatin (Murphy et al., 2002), which have been shown to inhibit M1 APs in *Arabidopsis* and other systems (Constam et al., 1995; Murphy et al., 2002). Meiotic Prophase Aminopeptidase (MPA1), an M1 AP, is important in meiotic chromosome segregation (Sanchez-Moran et al., 2004), and long-term exogenous application of puromycin to wild-type inflorescences results in phenotypes observed in *mpa1* (Sanchez-Moran et al., 2004) and *apm1* (presented here) loss-of-function mutants.

Previously, we showed that *APM1* is expressed at low levels in all vegetative tissues, at high levels in flowers, roots, and 5-d-old seedlings, and at intermediate levels in young rosette leaves (Murphy et al., 2002). This work examines *APM1* expression and protein subcellular localization patterns, the developmental phenotypes of loss-of-function mutations, and the effect of loss of *APM1* function on the localization of auxin transporters. Our results indicate that APM1 is a peripheral membrane protein associated with a noncanonical subcellular compartment, is a target of high concentrations of NPA, and functions in mechanisms other than meiosis and direct regulation of auxin transport.

RESULTS

APM1 Expression Is Developmentally Regulated

APM1 expression patterns were analyzed from embryogenesis through maturity, including gamete development, using native promoter:reporter fusions Pro*APM1*:green fluorescent protein

(GFP) and Pro*APM1*: β -glucuronidase (GUS) (Figure 1). At the early globular stage, a weak GFP signal was observed throughout the embryo (Figure 1A), but in the late globular stage, *APM1* expression was stronger in the epidermal and adjacent cells (Figure 1B). At the early heart stage, strong *APM1* expression was observed in the hypophysis and adjacent cells (Figure 1C) that are the site of root meristem formation (Jürgens, 2001). By the late heart stage, uniform expression was observed in the epidermal and ground tissue, root meristem, and suspensor (Figure 1D) (cell type classifications based on Jürgens, 2001). At the torpedo stage, the *APM1* expression was restricted to the vascular primordia (Figures 1E and 1F). In the mature embryo, GFP signals were observed in the vascular primordia throughout the hypocotyl/root axis and were no longer observed in the epidermis (Figures 1G and 1H). *APM1* expression patterns during embryogenesis suggest a role in the establishment of the root primordium, and the expression in the mature embryo suggests a role in postembryonic vascular development.

Consistent with previous RNA gel blot analyses (Murphy et al., 2002) and microarray data (see Supplemental Figure 1 online), *APM1* expression was greatest in 5-d-old seedlings, roots, rosette leaves, and flowers. Strong *APM1* expression using GUS and GFP reporters was observed in the elongation zone at the root tip (Figures 1I and 1O) and in the vascular tissue at the root-shoot junction (Figure 1J). *APM1* was expressed at the shoot apex (Figure 1K), discontinuously in the maturing vasculature in the cotyledon (Figure 1K), and in young rosette leaves and in the upper hypocotyl from 4 to 7 d after germination. In floral tissues, *APM1* was also strongly expressed in the anthers and ovules (Figures 1L and 1M). An autofluorescence control is shown in Figure 1N. *APM1* was strongly expressed in the vascular bundle and procambial tissue of 3.5- to 5-d-old root tips (Figure 1O) but decreased after 5 d to the point that expression was evident primarily in the provascular tissue (Figures 1P and 1Q). Moderate *APM1* expression was seen in root cap cells after 5.5 to 6 d (Figure 1P). In dark-grown seedlings, *APM1* expression was greatly reduced and was largely restricted to the vascular bundle (Figure 1R).

Mutational Analysis of *APM1* Function

A pictograph of *APM1* shows the promoter, start, exons, and introns with the position of the T-DNA insertion in the promoter of *apm1-1* and the ethane methanesulfonate (EMS)-generated mutations in *apm1-2* and *apm1-3* indicated by arrows (Figure 2A). After extensive backcrossing (five times), the expression of *APM1* in each line was analyzed by quantitation of steady state mRNA levels by quantitative real-time PCR. Expression of *APM1* in *apm1-1* homozygotes was 1 to 3% of the wild type (Figure 2B). *apm1-2* is an EMS mutant harboring a C-to-T base change at nucleotide position 2059, which results in the introduction of a stop codon at amino acid 687 (*APM1*^{R667}), and *APM1* expression in *apm1-2* heterozygotes was 40% of the wild type (Figure 2B). The *apm1-3* mutant is an EMS mutant with a C-to-T base change at position 2081 that results in an Ala-to-Val amino acid change at position 694 (*APM1*^{A694V}). *apm1-3* heterozygotes expressed a full-length transcript at 36% of wild-type levels (Figure 2B).

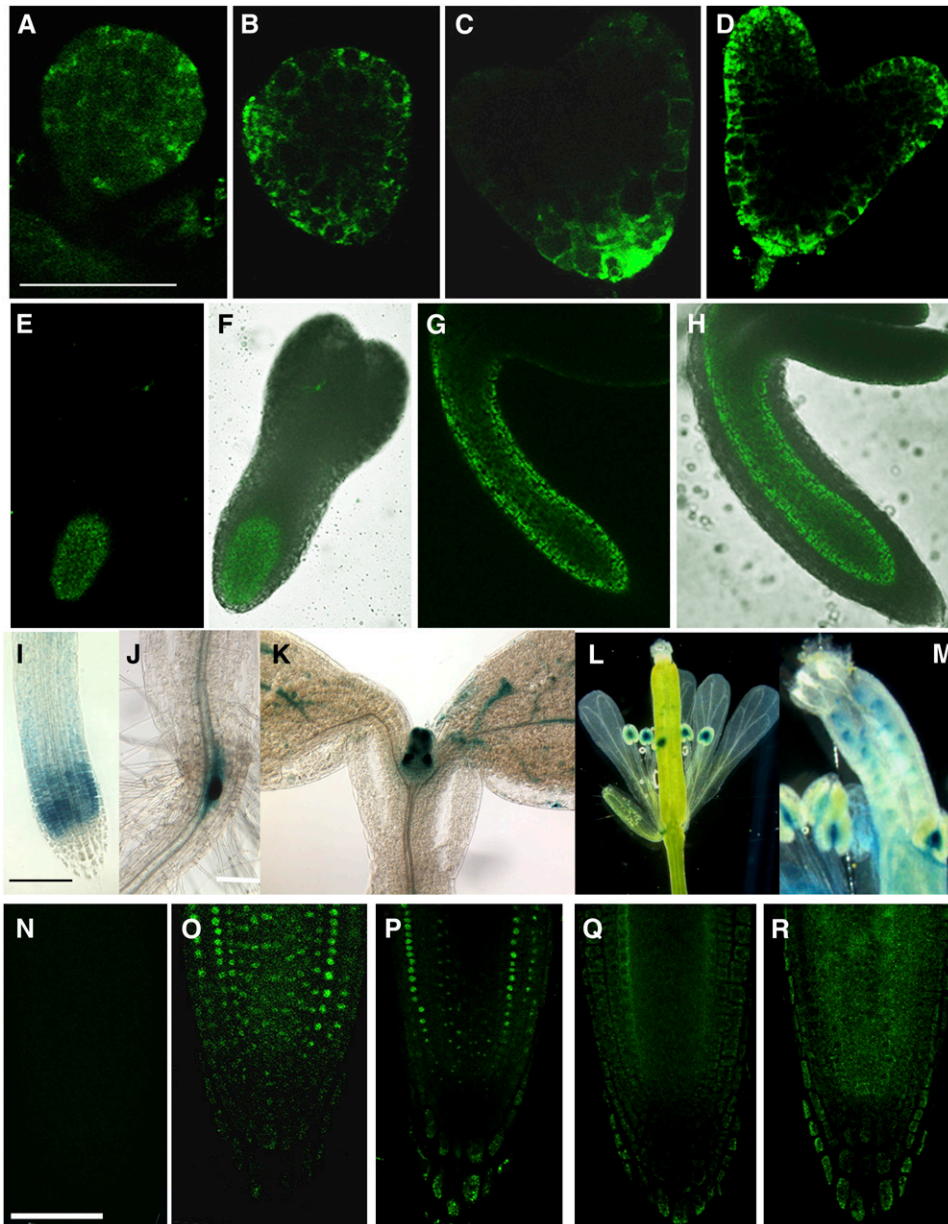


Figure 1. *APM1* Is Strongly Expressed during Embryogenesis, Organogenesis, and in Meristematic Regions.

(A) to (H) Pro*APM1*:GFP expression during *Arabidopsis* embryogenesis.

(A) Early globular stage.

(B) Late globular stage.

(C) Early heart stage.

(D) Late heart stage.

(E) Torpedo stage.

(F) Bright-field overlay of (E).

(G) Mature embryo.

(H) Bright-field overlay of (G).

(I) to (M) Pro*APM1*:GUS expression in the seedlings and flowers: root elongation zone (I), root-shoot transition zone (J), shoot apex (K), flowers (L), and anthers and ovules (M).

(N) to (R) Confocal laser scanning microscopy images of single sections. Pro*APM1*:GFP expression in seedlings.

(N) GFP autofluorescence control. The same settings were used for all GFP images.

(O) Five-day-old root tip.

A pictograph of the APM1 protein is presented in Figure 2C. The position of the catalytic motifs, protein-protein interaction motifs, and EMS mutation sites are indicated. Protein gel blot analysis of *apm1* mutants showed a very faint band in *apm1-1* ($-/-$) and faint bands in *apm1-1* ($+/-$) and *apm1-3* ($-/-$), as would be expected since none of the alleles are knockouts (Figure 2D; see Supplemental Figure 2 online). In *apm1-2* heterozygotes, both a full-length protein and an ~ 72 -kD band (APM1^{R667}) consistent with the predicted length of the truncated protein product were observed (Figure 2D). A loading control using antisera to the plasma membrane H⁺ ATPase is in Figure 2D, bottom panel.

Loss of APM1 Function Results in Embryonic Defects

APM1 is highly expressed during embryogenesis, especially in the hypophysis and vascular primordia (Figure 1; see Supplemental Figure 1 online), and developmental defects resulting from loss of APM1 function were observed during embryogenesis. In wild-type *Arabidopsis*, the first zygotic division gives rise to apical and basal daughter cells (Figure 3A). Embryonic defects in *apm1* can be observed at this stage with the absence or poor definition of an apical cell (Figures 3B and 3C). Subsequent divisions of the apical cell lead to the formation of the embryo proper, while the cell population derived from the basal cell gives rise to the filamentous embryo/suspensor (Figure 3D). Defects in these early divisions can also be observed with anticlinal division in the suspensor instead of the apical cell or asymmetric divisions in both apical and basal cells (Figures 3E to 3G). At the late globular stage, the suspensor cell adjacent to the embryo proper forms the lens-shaped hypophysis through a series of divisions and subsequently becomes the center for root meristem initiation in the wild type (Figure 3H). However, in *apm1* mutants, abnormal divisions or absence of divisions were observed in the hypophysis cells and cells adjacent to the hypophysis (Figures 3I to 3J). This suggests that the identity of the hypophysis was not established. More than fifty percent of the *apm1-1* and *apm1-2* and $\sim 30\%$ *apm1-3* embryos collapsed into a dense mass of tissue at the globular stage, resulting in embryo abortion.

In wild-type embryonic transition to the heart stage, the hypophysis undergoes another series of specialized divisions and becomes separate from the suspensor, and anticlinal divisions result in bilateral symmetry in the embryo proper (Figure 3K). At this stage, *apm1* mutants became swollen at the base of

the embryo proper, and the center for root meristem initiation could not be distinguished (Figures 3L and 3M). In $\sim 30\%$ of *apm1-1* and *apm1-2* mutants, these divisions were interrupted, giving rise to abnormal cotyledons. While the wild-type embryos progressed through to the torpedo stage, $\sim 20\%$ *apm1-1* and *apm1-2* mutants were arrested at the heart stage and consisted of undifferentiated, swollen masses of tissue. In some embryos, these tissues gradually underwent anticlinal divisions at the upper half to form the cotyledon primordia without forming the root meristem primordia.

Loss of APM1 Function in Seedlings and Adults

The primary roots of all three *apm1* allele mutants, both homozygotes and heterozygotes, stop elongating at 5 d after germination and the seedlings die, indicating that the mutants are haploinsufficient (Figures 4A to 4E). The severe *apm1-1* and *apm1-2* homozygotes are rootless (Figures 4A to 4E). The weak *apm1-3* ($+/-$ and $-/-$) mutant seedlings do not exhibit a rootless phenotype, consistent with the point mutation in this allele (APM1^{A694V}). Approximately twenty-five percent of *apm1-1* ($+/-$), *apm1-2* ($+/-$), and *apm1-3* ($+/-$ and $-/-$) seedlings can be rescued by inducing adventitious root formation from the hypocotyls, although a robust root system does not develop and the plants are susceptible to stress. However, in all rescued plants, the primary root does not extend and lateral roots are not formed, even if the plant grows to maturity. The *apm1-1* and *apm1-2* alleles must, therefore, be maintained as heterozygotes. All three alleles show a similar root arrest phenotype that appears to originate during embryogenesis, but APM1 appears to also be required in the seedling for survival.

Homozygous *apm1-1* and *apm1-2* seedlings also consistently exhibit a range of asymmetric, triple, cup-shaped, heart-shaped, and fused cotyledons (Figures 4B to 4E; see Supplemental Figure 3 online). However, the weaker allele, *apm1-3*, only shows a loss of symmetry (Figure 4A) and resembles the postgermination (nonembryonic) effects of NPA treatment (Murphy and Taiz, 1999a). Overall, the two severe alleles (*apm1-1* and *apm1-2*) show identical phenotypes, and the weak allele (*apm1-3*) exhibits similar but less severe phenotypes observed in the other two alleles.

Adult phenotypes of all three *apm1* alleles include a loss of apical dominance, reduced stature, delayed flowering (10 to 14 d after the wild type), small, incompletely filled siliques (due to

Figure 1. (continued).

(P) Six-day-old root tip.

(Q) Seven-day-old root tip.

(R) Four-day-old dark-grown seedling.

For these experiments, three GFP lines with ~ 50 seedlings per line were examined; nine GUS lines with 50 seedlings per line were examined. These patterns were observed in $>90\%$ of the individuals. The GFP lines showed similar expression tissue-specific patterns, including a line that showed nuclear envelope localization, shown in (N) to (R), because the line shows the results more clearly in seedling roots than the other lines. The relative expression is consistent with the microarray data (see Supplemental Figure 1 online). Bars = 100 μm in (A) and (B), 50 μm in (C) to (F), 25 μm in (G) and (H), 100 μm in (I) and (J), 200 μm in (K), 300 μm in (L), 100 μm in (M), and 50 μm in (N) to (R).

[See online article for color version of this figure.]

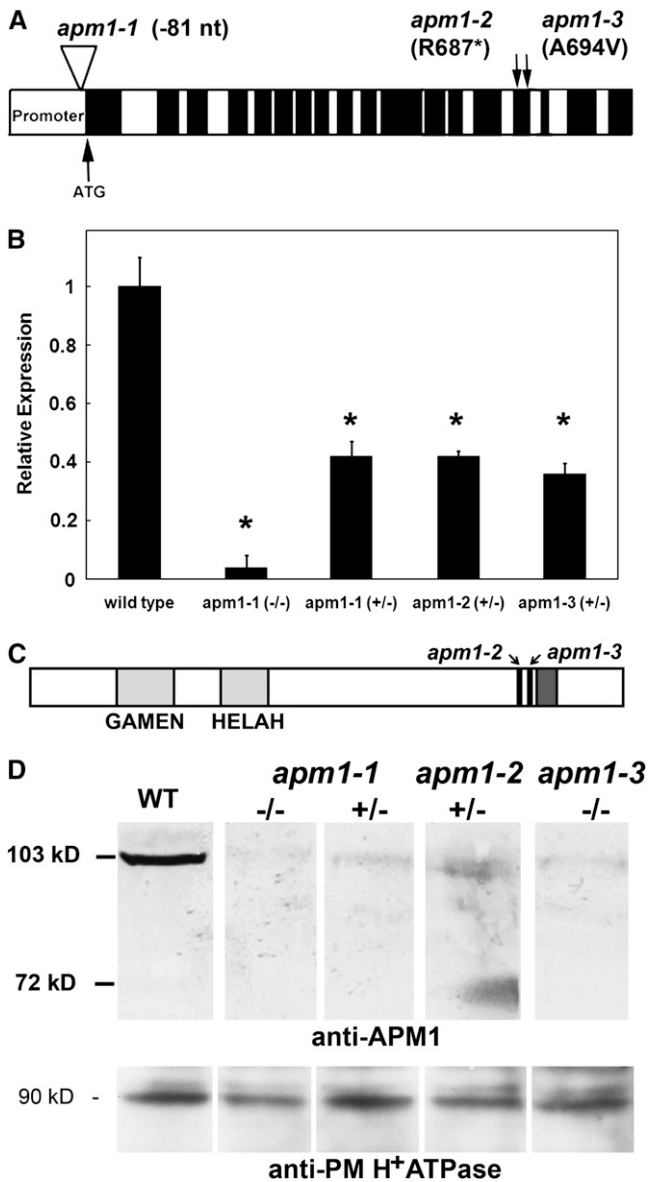


Figure 2. *APM1* Gene and Protein Maps.

(A) Map of *APM1* gene structure and mutation sites. Black boxes indicate exons, and white boxes indicate introns. The promoter is indicated N-terminal to the start site (ATG and an up arrow). The T-DNA insertion site in the promoter for *apm1-1* is indicated with an inverted triangle. The EMS point mutation sites in exon 15 for *apm1-2* and *apm1-3* are indicated with down arrows.

(B) Quantitative real-time PCR expression analysis in *apm1* mutants. Means and standard deviations from three independent experiments, true replicates were used, not subsamples (*t* test, * *P* < 0.001).

(C) Pictographic representation of the mutational sites for *apm1-2* and *apm1-3* (black lines with arrows) in relation to the catalytic (light-gray boxes with exopeptidase GAMEN and zinc binding HELAH) and protein-protein interaction (dark-gray box) motifs.

(D) Top panel: protein gel blot using anti-APM1 in wild-type and *apm1* alleles. None of the alleles are knockouts. A faint band can be observed in *apm1-1* (-/-) because it has 1 to 3% expression of APM1 compared

embryonic abortion), and delayed senescence (10 to 14 d after the wild type) compared with the wild type (Figure 4F). *apm1-2* (+/-) shows the greatest loss of apical dominance and stature, followed by *apm1-1* (+/-) and *apm1-3* (-/-). *apm1-1* alleles had comparable loss in silique filling (~20 to 30% filled), and higher growth temperatures resulted in more embryo abortions in *apm1-3*. *apm1* mutants also showed shorter stature under high light intensity.

The *apm1* seedling root, cotyledon, hypocotyls, and mature plant phenotypes (stature, apical dominance, silique size, silique filling, and senescence pattern) were complemented by transformation of *apm1-1* with Pro*APM1*:YFP-APM1 and Pro*APM1*:APM1-YFP (Figures 4G and 4H; see Supplemental Figure 3D online).

Since an arrested root growth phenotype and incompletely filled siliques were also observed in *apm1-1* and *apm1-2* heterozygotes and *apm1-3* homozygotes, we further analyzed the *apm1* mutants to determine if the mutation was recessive or dominant and if a meiotic defect was involved as is the case with *mpa1* (Sanchez-Moran et al., 2004). *apm1-1* heterozygotes were selfed, and progeny were genotyped and analyzed for root extension at 5 d. The expected genotypic ratio of 1 *APM1*/*APM1*:2 *APM1/apm1*:1 *apm1/apm1* for a recessive mutation was not observed (*P* < 0.001; Table 1), nor was the expected ratio for a recessive phenotypic mutation (3 wild type:1 mutant) observed. Instead, a segregation ratio of 1 wild type:2 mutant was observed, indicating that the mutation is partially dominant and that heterozygous individuals are haploinsufficient (*P* < 0.001; Table 1). Due to penetrance of the *apm1-1* (-/-) mutation (1 to 3% of wild-type *APM1* expression in surviving homozygous individuals), this allele is not 100% lethal. In addition, reciprocal crosses were made with wild-type and *apm1* heterozygotes. The expected ratio for a nonmeiotic mutation (1 *APM1*/*APM1*:1 *APM1/apm1*) was observed in both crosses (*P* > 0.05; Table 1). An additional 300 seedlings for each of the three crosses were scored for the arrested root phenotype, and the ratios of the wild type to mutant obtained were the same as the genotyped seedlings. In addition, no abnormal pollen germination or extension was observed in *apm1* alleles (data not shown). Unlike *MPA1* (Sanchez-Moran et al., 2004), *APM1* does not appear to function in meiosis.

with the wild type. Two bands can be seen in *apm1-2* (+/-), full-length and a truncated protein; the epitope that the antibody recognizes is contained in the truncated protein. *apm1-3* contains a point mutation that does not interfere with antibody recognition. The observed ~72-kD band in *apm1-2* heterozygotes is consistent with the predicted length of the truncated protein product based on the position of the introduced stop codon. Therefore, *apm1-1* has a very low level of full-length protein, *apm1-2* has a truncated protein that contains the catalytic domain but not the protein-protein interaction domains, and *apm1-3* has a full-length protein with a point mutation in a protein-protein interaction domain (*APM1*^{A694V}). Each lane contains 10 μg of total microsomal protein; an antibody to the C terminus of APM1 was used. Bottom panel: Loading control for the top panel. Each lane contains 10 μg of total microsomal protein; polyclonal antisera to the plasma membrane H⁺ATPase (PM H⁺ATPase) was used.

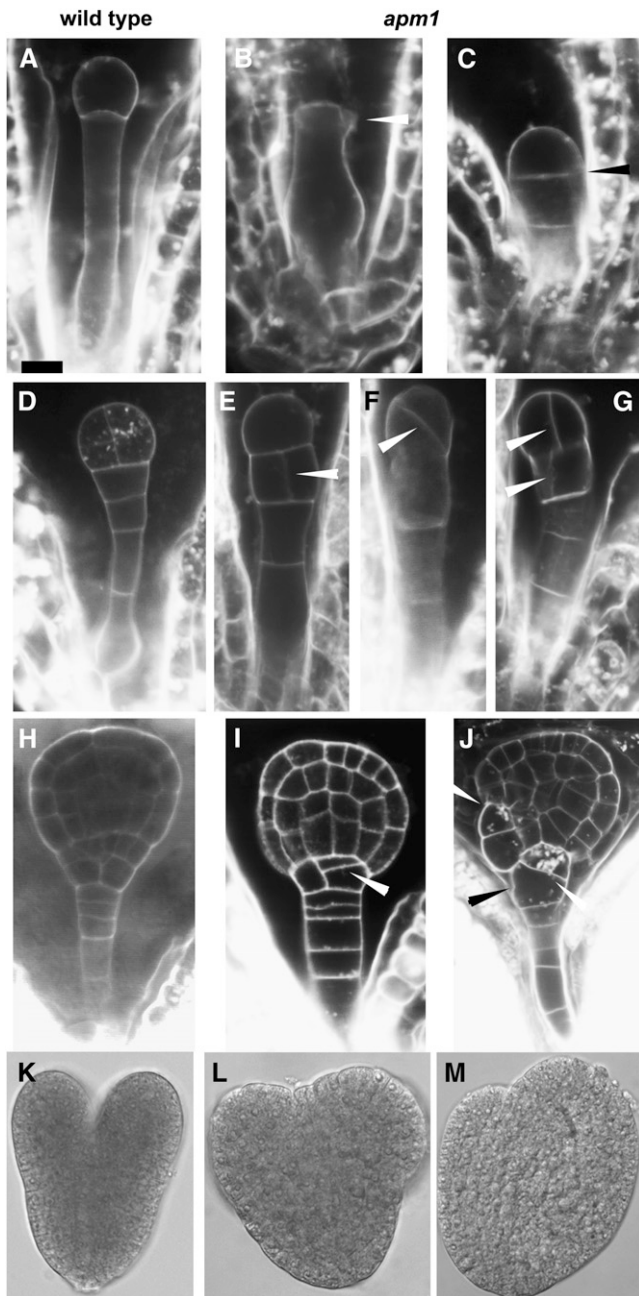


Figure 3. Loss of *APM1* Function Results in Embryonic Defects.

Representative images for each stage in embryogenesis are shown to emphasize that the described defects are common among all three independent alleles; for brevity, panels of each allele at each stage are not shown. All alleles were backcrossed at least five times (see Methods); therefore, it is unlikely that these phenotypes described below are related to an unlinked gene in each independent allele and because of the consistency of the defects observed among all the alleles.

(A) to (C) First zygotic division.

(A) Wild-type embryo with apical cell and basal cell.

(B) *apm1-1* missing the apical cell.

(C) *apm1-1* with poorly formed apical cell and basal cell with early division.

Further Analysis of *apm1* Root Phenotypes

We further investigated the root phenotype of *APM1* loss-of-function mutants. Lugol's staining of the starch grains in the root tip showed that the columella, root cap, and lateral root cap were not differentiated or organized into cell files in all three *apm1* alleles (Figures 5A to 5D). *ProcyclinB1;1::GUS* activity was not observed in the root meristem region of *apm1-1* heterozygotes or homozygotes (Figures 5E to 5G). Propidium iodide staining of cell walls also revealed abnormal planes of cell division in *apm1-1* roots (Figures 5H and 5I), similar to those observed during embryogenesis. The disorganization of the cell files and cessation of cell division suggest that the root meristem had prematurely switched to determinate growth, and propidium filling of meristematic cells indicated that these cells were dead.

Since *APM1* is strongly expressed in the root meristem in embryogenesis and the root cell files in all *apm1* mutants are disorganized, and all alleles (+/- and -/-) die at the seedling stage (unless manipulated to produce adventitious roots), we examined the quiescent center marker promoter traps QC-104 and QC-25 (Bechtold et al., 1993) in *apm1-1*. QC-104 GUS activity was reduced in *apm1-1* (+/-), and no GUS signal was observed in the *apm1-1* (-/-) roots (Figures 5J to 5L). Similarly, no QC-25 GUS activity was observed in *apm1-1* (-/-) roots (Figures 5M and 5N). This suggests that the disorganized cell files are a result of a collapsed quiescent center.

APM1 is also strongly expressed in the provascular tissue and metaxylem, so we examined root vascular tissue differentiation using a number of markers. First, we examined *apm1* mutants for expression of the *SHORTROOT* (*SHR*) and *SCARECROW* (*SCR*) transcription factors required for endodermal differentiation in root patterning (Sabatini et al., 2003; Cui et al., 2007). *SCR* restricts *SHR* movement, and *SHR* regulates *SCR* transcription. A Pro*SHR::GFP* signal seen in the stele of wild-type roots was restricted to the meristematic region in *apm1-1* (+/-) (Figures 5O and 5P), but the Pro*SHR::SHR-GFP* protein fusion was not observed in *apm1-1* (+/-) (Figures 5Q and 5R). A Pro*SCR::GFP* signal visible in the endodermis of wild-type roots was also not

(D) to (G) Two-cell embryo proper.

(D) Wild-type embryo with symmetric radial division in apical cell.

(E) *apm1-3* with anticlinal division in suspensor below apical embryo.

(F) *apm1-2* with asymmetric radial division in apical embryo.

(G) *apm1-3* with asymmetric radial division in apical embryo and anticlinal division in the adjacent suspensor cell.

(H) to (J) Late globular embryo.

(H) Wild-type embryo.

(I) *apm1-1* embryo has asymmetric anticlinal division in the hypophysis and an additional division periclinal to the suspensor.

(J) *apm1-2* embryo has asymmetric divisions in the hypophysis, adjacent suspensor and adjacent epidermal cells.

(K) and (L) Heart-stage embryo.

(K) Wild-type embryo shows bilateral symmetry and cotyledon primordia.

(L) and (M) *apm1-2* shows asymmetric cotyledon primordia and poorly defined root primordia.

Bars = 5 μ m **(A) to (J)** and 50 μ m **(K) to (M)**. Arrowheads indicate aberrant planes of cell division.

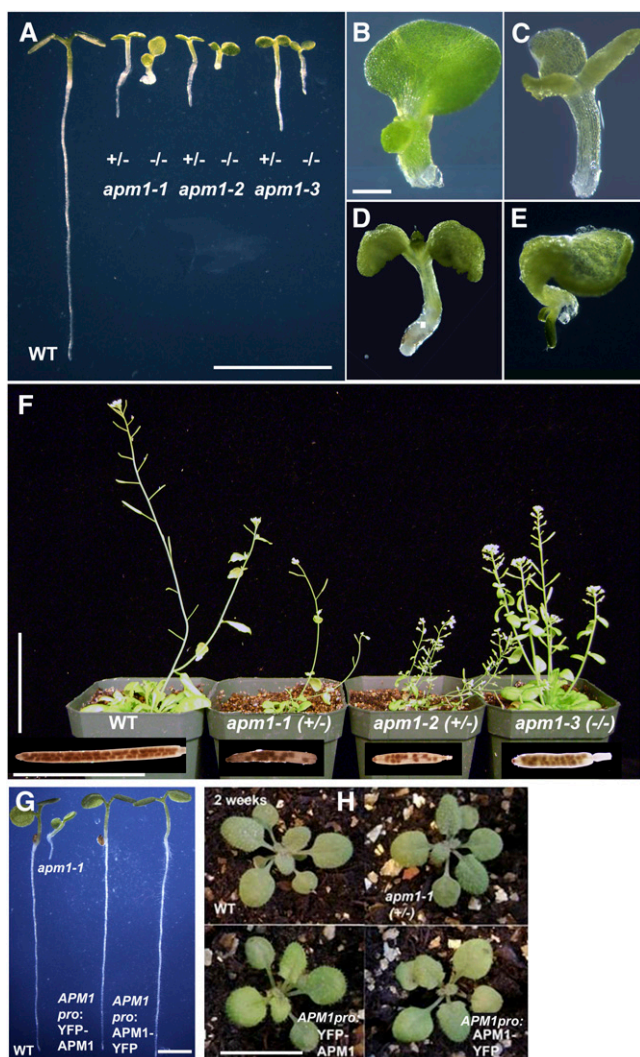


Figure 4. Loss of *APM1* Function in Seedlings and Adults.

(A) Wild-type and *apm1* heterozygous and homozygous mutants and 5-d-old seedlings.

(B) *apm1-1* ($-/-$) seedling.

(C) *apm1-1* ($-/-$) seedling.

(D) *apm1-2* ($-/-$) seedling.

(E) *apm1-2* ($-/-$) seedling.

(F) Wild-type and *apm1* alleles, 4-week-old plants, and siliques.

(G) Wild type, *apm-1-1*, and *apm1-1* transformed with either Pro*APM1*:YFP-*APM1* or Pro*APM1*:*APM1*-YFP at 5-d, showing complemented root phenotype.

(H) Wild type, *apm-1-1*, and *apm1-1* with either Pro*APM1*:YFP-*APM1* or Pro*APM1*:*APM1*-YFP at 2 weeks. *apm1-1* and *apm1-3* transformed with Pro*APM1*:YFP-*APM1* or Pro*APM1*:*APM1*-YFP displayed a wild-type phenotype, including secondary root formation. *apm1-2* (containing a truncated protein) did not display full complementation when transformed with either Pro*APM1*:YFP-*APM1* or Pro*APM1*:*APM1*-YFP. Bars = 5 mm in (A), 200 μ m in (B) to (E), and 3 cm in (F) to (H).

[See online article for color version of this figure.]

observed in *apm1-1* mutants (Figures 5S and 5T). However, ectopic localization of Pro*SCR*:GFP signal was observed in the epidermis (Figure 5U). This lack of wild-type *SCR* and *SHR* expression is consistent with the absence of lateral roots in *apm1* mutants.

BETA-XYLOSIDASE1 (*BXL1*) is expressed in protoxylem and xylem parenchyma cells (Goujon et al., 2003). No expression of Pro*BXL1-1*:GUS activity was observed in *apm1-1* (Figures 5V and 5W). In cross sections, the root vascular tissue in *apm1-1* and *apm1-2* was observed to be smaller, the cell types less differentiated, and the xylem poles lacked bilateral symmetry compared with the wild type (Figure 5X). The vascular tissue in the weak allele, *apm1-3*, was less irregular than in the other two mutants but had increased cell number in the stele (Figure 5X). These results indicate that *APM1* is required for postembryonic vascular transition and maturation in the seedling root.

Analysis of *apm1* Shoot Phenotypes

In addition to the phenotypes noted above, shoot phenotypes were observed in *apm1* mutants. Similar to the observation made in roots, no Pro*cyclinB1;1*:GUS activity was observed at the shoot apex in *apm1-1* 5-d-old seedlings (Figures 6A and 6B). Although vascular patterning was disrupted in the root, cotyledons and leaves in *apm1* appeared to have continuous, but fewer, wild-type-like vasculature traces (see Supplemental Figure 8 online). However, aberrant trichome branching was also noted in *apm1-1* and *apm1-2* and less frequently in *apm1-3* (Figures 6C and 6D).

The most prominent shoot phenotype occurs in the hypocotyls. Hypocotyls of *apm1-1* and *apm1-2* exhibited enlarged epidermal cells with apparent cell adhesion defects (Figures 6E and 6F). However, like the cotyledon defects, the hypocotyl epidermal cell expansion defect was not observed in *apm1-3*. A defect in secretion could underlie this observation, as ruthenium red staining of mucilage from imbibed seeds is also altered in *apm1* mutants (see Supplemental Figure 3 online).

Inducible Silencing of *APM1*

The haploinsufficiency observed in *apm1* mutants suggests that dosage effects play a role in the observed phenotypes. *APM1*-inducible artificial microRNA constructs were made using pOpOff vectors, and pOpOff lines were generated by floral dip of Columbia-0 (*Col-0*) ecotype (see Methods). pOpOff and pOpOn vectors provide for stringent and quantitative transgene expression when induced by dexamethasone (Dex) that can be used to investigate gene expression dosage effects (Craft et al., 2005; Moore et al., 2006; see Supplemental Figure 4 online). While 1 μ M Dex had no apparent negative effects, seeds germinated and grown on 2 to 5 μ M Dex had reduced primary root length at 5 d and exhibited asymmetric but not fused or excess cotyledons ($P < 0.05$; Figure 7A; see Supplemental Figure 4A to 4C online). Silencing induced by 6 μ M Dex resulted in a root phenotype similar to the weakest allele of *apm1* (*apm1-3* heterozygotes). More severe *apm1* root phenotypes were reproduced in seedlings grown on 8 or 10 μ M Dex ($P < 0.001$; Figure 7A; Supplemental Figure 4A-C online). The *apm1* incompletely filled silique

Table 1. Genetic Analysis of *apm1-1* Segregation Ratios

Hypothesis	Progeny			Recessive	Partial Dominance
	Genotype				
	Wild Type	<i>apm1-1</i> (+/-)	<i>apm1-1</i> (-/-)	χ^2	χ^2
Parents					
<i>APM1/apm1</i> × <i>APM1/apm1</i>	34	63	3	1:2:1 25.98 ^{a, h}	2:1 0 ^b
<i>APM1/apm1</i> × <i>APM1/APM1</i>	41	59		1:1 3.242 ^c	1:1 3.242 ^c
<i>APM1/APM1</i> × <i>APM1/apm1</i>	46	54		1:1 0.64 ^c	1:1 0.64 ^c
Phenotype					
	Wild Type	<i>apm1</i>		χ^2	χ^2
Parents					
<i>APM1/apm1</i> × <i>APM1/apm1</i>	34	66		3:1 89.65 ^{d, h}	2:1 0 ^e
<i>APM1/apm1</i> × <i>APM1/APM1</i>	41	59		∞ :0 ^f –	1:1 3.242 ^g
<i>APM1/APM1</i> × <i>APM1/apm1</i>	46	54		∞ :0 ^f –	1:1 0.64 ^g

^aProbability for a recessive trait calculated by χ^2 test with 1 *APM1/APM1*:2 *APM1/apm1*:1 *apm1/apm1* segregation ratio. *df* = 2. The expected ratio was not obtained.

^bProbability for partial dominant trait calculated by χ^2 test with 2 *APM1/apm1*:1 *APM1/APM1* segregation ratio. *df* = 2. The expected ratio was obtained.

^cProbability calculated by χ^2 test with 1 *APM1/APM1*:1 *APM1/apm1* segregation ratio for a meiotic defect. *df* = 1. The expected ratio was obtained. The recessive/partial dominance hypotheses cannot be distinguished in this test.

^dProbability calculated by χ^2 test with 3 wild type:1 mutant segregation ratio. *df* = 1. The expected ratio was not obtained.

^eProbability calculated by χ^2 test with 2 mutant:1 wild type segregation ratio. *df* = 1. The expected ratio was obtained.

^fAll wild type:no mutant (∞ :0) segregation ratio expected. *df* = 1. The expected ratio was not obtained.

^gProbability calculated by χ^2 test with 1 wild type:1 mutant segregation ratio for a meiotic defect. *df* = 1. The expected ratio was obtained.

^h*P* < 0.001.

One-hundred seedlings were genotyped using PCR for each cross presented. The expected segregation ratio was not obtained for *APM1/apm1* × *APM1/apm1*. However, the reciprocal crosses to the wild type showed the expected ratios. Seedlings were also scored for root extension phenotype.

(embryonic abortion) phenotype could also be induced with application of Dex to the pOpOff *APM1* transformants and paralleled the concentration effects observed on the root length phenotype, with significantly fewer seeds produced after 5 to 10 μ M Dex induction (*P* < 0.05; Figure 7B; see Supplemental Figure 4A to 4C online). Seedlings that germinated from the pOpOff plants with 10 μ M Dex treatment showed the abnormal cotyledons observed in *apm1-1* and *apm1-2* mutants. However, the arrested root phenotype was only observed if the seedlings were germinated on plates supplemented with Dex. Quantitative real-time PCR analysis after 8 or 10 μ M Dex induction in 5-d-old seedlings showed that *APM1* expression was suppressed to *apm1* (+/-) levels (Figure 2B; see Supplemental Figure 4A to 4C online).

Developmental analyses indicated that *APM1* function is required for both embryonic development and postembryonic root meristem development. To further refine the developmental time point at which *APM1* gene expression is required for proper root development, a time course for inducible silencing was conducted (Figures 7C and 7D). The *apm1* arrested root phenotype was observed when *APM1* gene expression was silenced for the

first 3 d following germination, consistent with the increase in *APM1* expression that begins at day three and its proposed role in maintenance of the root meristem. Importantly, the *apm1* arrested root phenotype was reproduced when *APM1* was silenced in wild-type seedlings, which have no prior embryonic defects.

Inducible Expression of *APM1*

The effects *APM1* dosage on *apm1* phenotypes were also investigated using inducible expression. *APM1*-inducible expression constructs were made with Dex-inducible pOpOn vectors (Moore et al., 2006), and pOpOn lines were generated by floral dip of *apm1-1* (see Methods). While increased primary root length was observed at all Dex concentrations, primary root length was restored to wild-type-like length at 10 μ M Dex (*P* > 0.05; Figure 7E; see Supplemental Figure 4D to 4F online). The incompletely filled silique phenotype was restored at 8 or 10 μ M Dex (Figure 7F; see Supplemental Figure 4D to 4F online), as was wild-type senescence. Seedlings (*apm1-1* genotype) that

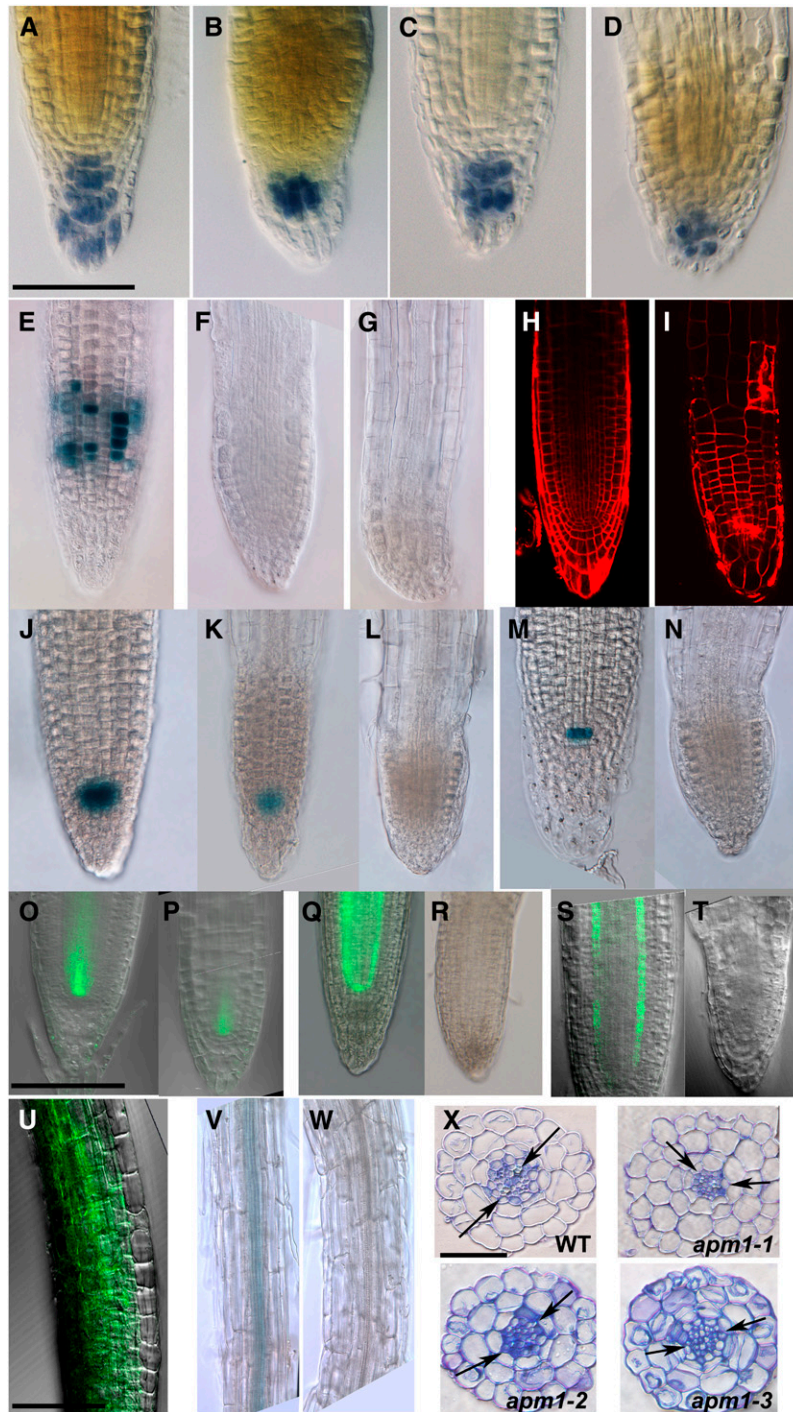


Figure 5. Root Phenotypes of *APM1* Loss-of-Function Mutants.

(A) to (D) Starch granules in 5-d-old root stained with Lugol's. Wild type (A), *apm1-1* (+/-) (B), *apm1-2* (+/-) (C), and *apm1-3* (-/-) (D). The columella cells are disorganized in *apm1* mutants.

(E) *ProCyclinB1;1:GUS* root.

(F) *ProCyclinB1;1:GUS* in *apm1-1* (+/-) root.

(G) *ProCyclinB1;1:GUS* in *apm1-1* (-/-) root. CyclinB is a marker for cell division, and cell division appears to cease in *apm1* mutants, consistent with arrested root growth.

(H) Wild type root stained with propidium iodide.

germinated from 10 μ M Dex-induced pOpOn siliques did not show the abnormal cotyledons observed in *apm1*. However, the arrested root phenotype was observed if the seedlings were grown without Dex and was rescued when grown on plates supplemented with Dex. Quantitative real-time PCR analysis after 10 μ M Dex induction in 5-d-old pOpOn seedlings showed that *APM1* expression was at wild-type levels ($P = 0.1$; see Supplemental Figure 4D to 4F online).

A time course for inducible expression was conducted (Figures 7G and 7H). The length of the induction period corresponded to the length of the primary root. The *apm1* arrested root phenotype was rescued when *APM1* gene expression was induced for 5 d (Figure 7G). When *APM1* expression was induced at 4 or 5 d after germination, then the root phenotype was rescued (Figure 7H). As controls, Figure 7I shows 5-d-old wild type and *apm1-1* grown in the presence and absence of Dex. Wild-type lines transformed with pOpOff *GFP* did not exhibit the *apm1-1* arrested root phenotype after Dex induction (Figure 7J). *apm1-1* lines transformed with pOpOn *GFP* did not show a wild-type root phenotype after Dex induction (Figure 7K).

These inducible silencing and expression data indicate that, in addition to a function in embryonic development, there is a critical time point at 3.5 to 4 d after germination where *APM1* is necessary for primary root meristem maintenance.

Auxin-Related Phenotypes of *APM1* Loss-of-Function Mutants

APM1 Gene Expression Is Auxin Responsive

Treatment with indole-3-acetic acid (IAA) resulted in enhancement and upward extension of the Pro*APM1*:GFP signal in the vascular bundle and a loss of signal in the epidermal and cortical cells (Figures 8A and 8B). Quantitative real-time PCR indicated a

2.5-fold increase in *APM1* expression after a 30-min IAA treatment and a fourfold increase after 2 h (see Supplemental Figure 5 online). Treatment with 2,4-D, a poorly transported artificial auxin, resulted in a decrease in the vascular Pro*APM1*:GFP signal (Figure 8C). Treatment of 5-d-old Pro*APM1*:GFP seedlings with 50 μ M abscisic acid or 15 μ M jasmonic acid for 2 h had no effect on *APM1* expression (data not shown).

Auxin-Induced Gene Expression Is Altered in *apm1* Mutants

DR5 is an artificial auxin reporter derived from the natural auxin-responsive promoter *GH3* and indicates auxin concentrations in the 10^{-6} to 10^{-4} μ M range (Ulmasov et al., 1997), and the *IAA2* reporter contains 425 bp of the auxin-responsive *IAA2* promoter (Swarup et al., 2001). In the wild type, Pro*IAA2*:GUS activity was observed in the vascular tissue of the primary leaves and shoot apex, while in *apm1*, no GUS activity was observed (Figures 8D and 8E), suggesting decreased auxin production or enhanced auxin transport out of the shoot apex in *apm1*. In the wild type, Pro*DR5*:GUS activity was observed at the quiescent center, initials, and columella and extended into the vascular tissue (Figure 8F). In *apm1-2* crosses with Pro*DR5*:GUS, increased GUS activity was observed in the root apex, although no GUS activity was seen in the columella as these cell types are poorly defined in *apm1* loss-of-function mutants (Figure 8G). In *apm1-1* crosses to Pro*DR5*:GFP, the GFP signal in *apm1* was enhanced at the root apex compared with the wild type (Figures 8H and 8I), suggesting that basipetal redirection of auxin is impaired in the mutant.

Auxin Transport Is Altered in *apm1*

Direct measurement of auxin transport is usually performed in 5- to 6-d-old *Arabidopsis* seedlings (Murphy et al., 2000; Geisler et al., 2003, 2005; Peer et al., 2004; Terasaka et al., 2005;

Figure 5. (continued).

- (I) *apm1-1* (+/–) root stained with propidium iodide. Planes of cell division are altered in *apm1* seedlings as in *apm1* embryos.
 - (J) QC-104 shows GUS staining in the quiescent center (QC).
 - (K) QC-104 in *apm1-1* (+/–) shows faint staining in the QC.
 - (L) QC-104 in *apm1-1* (–/–) shows no staining in the QC.
 - (M) QC-25 shows GUS staining in the QC.
 - (N) QC-25 in *apm1-1* (–/–) shows no staining in the QC. The QC appears to be inactive in *apm1* mutants.
 - (O) Pro*SHR*:GFP.
 - (P) Pro*SHR*:GFP in *apm1-1* (+/–) shows restricted expression near the meristematic regions.
 - (Q) Pro*SHR*:SHR-GFP is expressed in the stele.
 - (R) Pro*SHR*:SHR-GFP in *apm1-1* (+/–) shows no signal.
 - (S) Pro*SCR*:GFP signal in vascular strands.
 - (T) Pro*SCR*:GFP in *apm1-1* (–/–) shows no signal in the vascular tissue.
 - (U) Ectopic expression of Pro*SCR*:GFP in *apm1-1* (+/–) in epidermal cells. This is also observed in *apm1-1* (–/–) (see Supplemental Figure 8 online). The ground tissue specifiers *SCR* and *SHR* are misexpressed/mislocalized in *apm1* mutants.
 - (V) Pro*BXL1-1*:GUS shows staining in the xylem parenchyma.
 - (W) Pro*BXL1-1*:GUS in *apm1-1* (+/–) shows no staining, indicating that these cells have altered cell identity.
 - (X) Root cross section stained with toluidine blue; arrows point to xylem poles. *apm1-1* (+/–), *apm1-2* (+/–), and *apm1-3* (–/–). The xylem poles are not opposite each other in *apm1* mutants, the vascular tissue appears to have a greater number of smaller cells than does the wild type, and additional cortical cells are observed. For the Pro*cylinB1*:GUS reporter, 100 seedlings were observed, with the results presented observed in all seedlings. For the QC:GUS and Pro*BXL1-1*:GUS reporters, 50 seedlings were observed, with the results presented observed in all seedlings. For the GFP reporters and fusions, 30 seedlings were observed, with the results presented observed in all seedlings.
- Bars = 100 μ m in (A) to (V) and 50 μ m in (X).

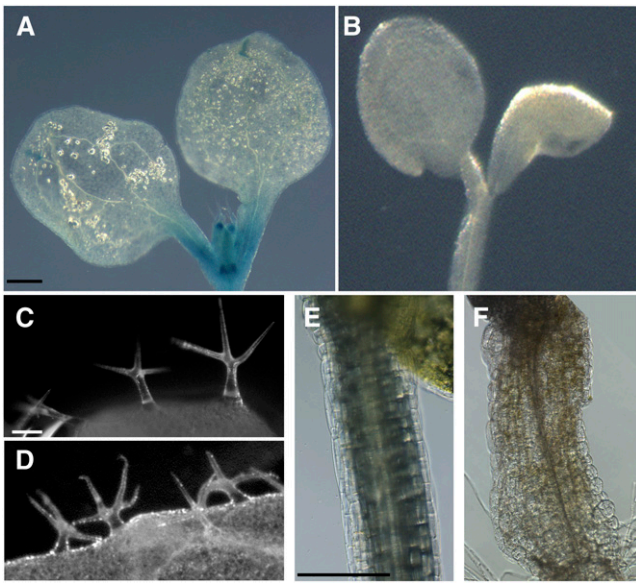


Figure 6. Shoot Phenotypes of *APM1* Loss-of-Function Mutants.

- (A) *ProCyclinB1;1:GUS* in shoot tip of 5-d-old seedling.
 (B) *ProCyclinB1;1:GUS* in *apm1-1 (+/-)* shows no staining in 5-d-old shoot tip.
 (C) Wild-type trichomes.
 (D) *apm1-1 (+/-)* trichomes show additional branching and hooking at the tips.
 (E) Wild-type hypocotyls.
 (F) *apm1-1 (+/-)* hypocotyl epidermal cells show cell adhesion and cell expansion defects.
 Bars = 200 μm in (A) and (B), 100 μm in (C) and (D), and 200 μm in (E) and (F).
 [See online article for color version of this figure.]

Blakeslee et al., 2007; Peer and Murphy, 2007). In *apm1-3*, basipetal auxin transport out of the shoot apex was significantly enhanced compared with the wild type ($P < 0.02$; Figure 9A), while basipetal transport from the root apex was significantly reduced in the first 2 mm from the root tip ($P < 0.01$; Figure 9A). These results are consistent with auxin reporter results and indicate that *APM1* negatively regulates auxin transport in the shoot apex and positively regulates auxin transport upwards from the root tip.

Gravitropism Is Altered in *apm1*

Consistent with *APM1*-positive regulation of root basipetal transport, gravitropic bending was also slower in the *apm1-1 (+/-)* and *apm1-2 (+/-)* mutants compared with the wild type ($P < 0.01$; Figure 9B). Gravitropism in *apm1-3 (-/-)* was not different from in the wild type, after 9 h of gravistimulation, but the rate is a result of decreased linear growth in the *apm1-1* and *apm1-2* heterozygotes compared with the *apm1-3* homozygote. *apm1-1* and *apm1-2* heterozygotes were used for these experiments because the homozygous seedlings do not have roots (Figures 3A to 3E).

After gravitropic stimulus, auxin transported from the root tip to the elongation zone is asymmetrically redirected to the lower root

surface in reference to the gravity vector (Wisniewska et al., 2006; Peer and Murphy, 2007). A similar asymmetric change in *APM1* expression was observed after gravity stimulus, with expression enhanced in the epidermal and cortical cells on the upper side and absent on the lower side (Figure 9C). These results are consistent with the loss of *APM1* expression seen in epidermal root cells treated with 10 nM IAA and suggest that *APM1* expression is negatively regulated by IAA levels in epidermal and cortical cells at the root tip and is positively regulated in vascular tissues in the same region.

APM1 Subcellular Localization by Transmission Electron Microscopy

Transmission electron microscopy immunolocalization analyses of high pressure freeze-substituted 5-d-old seedlings was used to investigate the subcellular localization of *APM1* (Figure 10). Studies were conducted using both the C terminus and peptide *APM1* antisera with identical results. In cortical root cells, *APM1* was observed on the margin of Golgi cisternae and plasma membrane (Figures 10A and 10B) as well as in discrete regions of some multivesicular bodies (Figure 10C).

In maturing cells, discrete aggregations of *APM1* were found at the tonoplast and within electron-dense intravacuolar bodies (Figures 10D and 10E). *APM1* signals were seen at the plasma membrane in cells adjacent to differentiating vascular tissue (Figures 10F and 10G). *APM1* was also associated with intracellular cross walls and fragments of collapsing cellular structures in differentiating metaxylem elements (Figures 10F to 10I), consistent with *APM1* Δ (truncated *APM1*) observation in the cell wall debris (Murphy et al., 2002). Preimmune serum controls using 2 \times concentration showed very low signal on the cell walls and in the cytoplasm of the root (see Supplemental Figure 6 online).

APM1 Subcellular Localization by Immunohistochemistry and Protein Fusions

APM1 has a hydrophobic subdomain characteristic of peripheral membrane proteins and was previously purified from plasma membrane, microsomal, and soluble fractions (Murphy et al., 2002). Previously, it was thought that it was also glycosylated, but this was due to a comigrating band. Immunolocalizations, visualization of *ProAPM1:YFP-APM1* translational fusions, and protein gel blot analyses of subcellular fractions all indicate the presence of *APM1* in both cytosolic and endomembrane compartments (Figure 11; see Supplemental Figure 2 online). *APM1* immunolocalization (with two different purified antisera) and *ProAPM1:YFP-APM1* (and *Pro35S:YFP-APM1*; see Supplemental Figure 8 online) signals were seen only in cells and tissues where expression of *APM1* was seen in promoter fusions; autofluorescence corresponding to Alexafluor 488 or yellow fluorescent protein (YFP) was not observed in *apm1-1* or the wild type, respectively (see Supplemental Figure 2A and 3 online). However, *apm1-1 (+/-)* transformed with *Pro35S:YFP-APM1* appeared to grow to maturity faster than the wild type (see Supplemental Figure 3D online). *APM1-YFP* C-terminal fusion transformants were also analyzed, which showed no signal, but complemented *apm1-1* (see Methods).

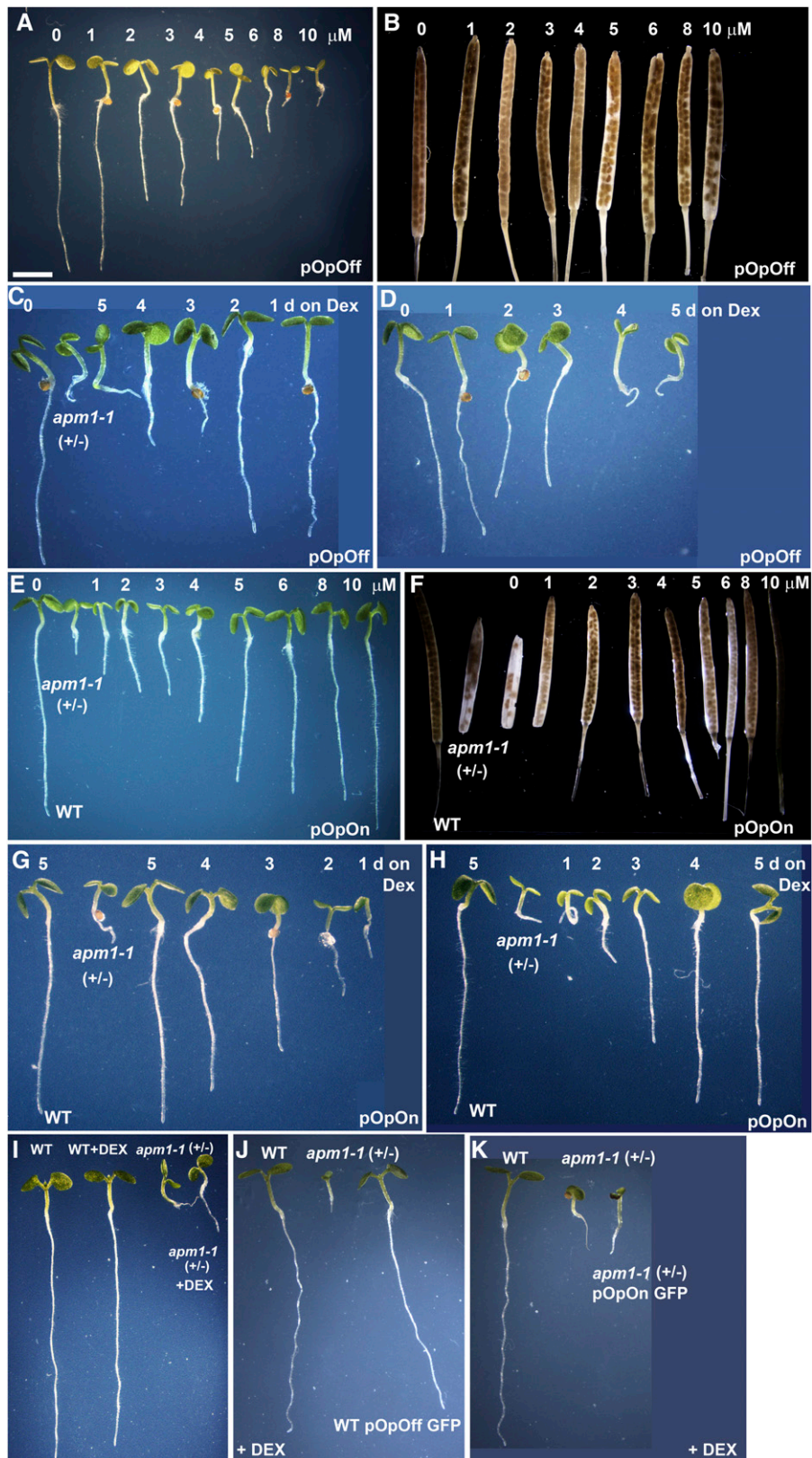


Figure 7. Inducible Silencing and Expression of *APM1*.

Signals from APM1 immunolocalization and N-terminal YFP fusions of APM1 were associated with endomembrane structures and the plasma membrane in cortical and epidermal cells (Figures 11A to 11L). In roots, APM1 was also observed in the stele and was abundant in metaxylem and epidermal cells (Figures 11A to 11C and 11H). This pattern was reiterated in the lateral roots (Figure 11L). The signal was primarily punctate and intracellular (Figures 11D to 11F). At the shoot apex where *APM1* is strongly expressed, APM1 signals were observed in the cytosol and at the plasma membrane of the epidermis, unexpanded primary leaves, and meristem region, and in epidermal cells of the hypocotyl (Figures 11I and 11J). In adult plants, APM1 was observed in the transitional meristem (Figure 11K), consistent with microarray data (see Supplemental Figure 1 online). APM1 was also observed at the cell plate of newly divided cells in the root and shoot apices (Figures 11B, 11C, 11G, 11J, and 11K).

In order to verify the mixed membrane and cytosolic association of APM1, microsomal membranes were prepared from 5-d-old *Arabidopsis* seedlings, differentially solubilized, and analyzed by protein gel blot analysis with the APM1 peptide antiserum. As was seen previously with the C-terminal APM1 antisera (Murphy et al., 2002), full-length APM1 (103 kD) and a 42-kD APM1 C-terminal degradation product (previously described and sequenced in Murphy et al. [2002] as APM1 Δ and sequenced again here) were detected in the 8000 g and 100,000 g supernatants and 100,000 g pellets, although only a small amount of the degradation product was present in the 100,000 g pellet (42 kD) (see Supplemental Figure 2F online). Consistent with APM1 being associated with the membrane, full-length APM1 (103 kD) could be released from the 100,000 g microsomes with 0.1 M Na₂CO₃, while Triton X-100 and SDS pretreatment enhanced release of APM1 from the 100,000 g pellet compared with SDS sample buffer alone (see Supplemental Figure 2F online). By contrast, the plasma membrane marker AHA2 could only be displaced from membranes by Triton X-100 and SDS pretreatment, while a soluble protein, APP1, was only found in soluble fractions, and its localization was not altered by pretreatments (see Supplemental Figure 2F online). These results indicate that

APM1 is a peripheral membrane (rather than a type II membrane-anchored) protein and that a subpopulation of APM1 is more easily displaced from membranes.

Microsomes from 5-d-old wild-type *Arabidopsis* seedlings were fractionated on a 14 to 55% linear sucrose gradient and analyzed by protein gel blots with antibodies against APM1 and subcellular compartment markers (Figure 11M). APM1 was observed primarily in lighter fractions (23.5 to 24.6% sucrose) but continued to be detected in all sucrose densities to 43.6%. The lower quantities of APM1 in higher density fractions partially overlapped with the endosomal marker Pep12 and, to a lesser extent, both the vacuolar marker Syp22 and the plasma membrane marker AHA2 (39.2 to 43.6%). APM1 was absent in fractions containing the endoplasmic reticulum marker Sec12 or the *trans*-Golgi network marker Syp41. No marker analyzed exhibited the same sedimentation as the fractions containing the majority of APM1. This result is similar to that observed with M1 insulin-responsive AP IRAP, which characterizes unique light membrane fractions in mammals (Lim et al., 2001; Fernando et al., 2007). The sucrose gradient of the light membrane fraction was analyzed for lipid content (Kunst et al., 1988) and exhibited an ~30% increase in C24 and C26 fatty acids compared with whole microsomal membranes (Table 2), consistent with increased sphingolipid content. In addition, diacyldiglycerol and a slightly more mobile lipid in thin layer chromatography separations were depleted in the light membrane fractions compared with microsomal membranes, similar to decreases reported in detergent-resistant membranes derived from total plasma membrane fractions (Mongrand et al., 2004).

Trafficking Inhibitors Alter APM1 Localization

Trafficking inhibitors have been used to study the subcellular localization of proteins to elucidate the membrane compartment (s) in which they reside. Since APM1, a peripheral membrane protein with both cytosolic and membrane association is found in light membrane fractions, we examined the effects of inhibitors on its localization. Precedents for using trafficking inhibitors to support peripheral membrane protein localization were

Figure 7. (continued).

Inducible silencing of *APM1* phenocopies *apm1*. Wild type transformed with the pOpOff artificial microRNA *APM1* construct.

(A) and (B) Dosage effect of silencing *APM1* in 5-d-old seedling (A) and silique (B) development.

(C) Seeds germinated on plates without 10 μ M Dex were subsequently transferred to plates supplemented with 10 μ M Dex for 5, 4, 3, 2, or 1 d to induce *APM1* silencing.

(D) The reciprocal experiment was also performed whereby plants were first germinated on 10 μ M Dex for 1, 2, 3, 4, or 5 d and then transferred to plates without the induction medium. Inducible expression of *APM1* complements *apm1*. *apm1-1* (+/-) transformed with the pOpOn *APM1* construct

(E) and (F) Dosage effect on expressing *APM1* in 5-d-old seedling (E) and silique (F) development.

(G) Seeds were germinated on plates without Dex and then transferred to plates supplemented with 10 μ M Dex for 5, 4, 3, 2, or 1 d to induce *APM1* expression.

(H) The reciprocal experiment was also performed whereby plants were first germinated on 10 μ M Dex for 1, 2, 3, 4, or 5 d prior to transfer to plates without Dex.

(I) Wild type and *apm1-1* (+/-) without and with 10 μ M Dex for 5 d.

(J) Wild type, *apm1-1* (+/-), and wild type transformed with pOpOff GFP grown on with 10 μ M Dex for 5 d.

(K) Wild type, *apm1-1* (+/-), and *apm1-1* (+/-) transformed with pOpOn GFP with 10 μ M Dex for 5 d.

Bars = 5 mm in (A), (C) to (E), and (G) to (K) and 3 cm in (B) and (F).

[See online article for color version of this figure.]

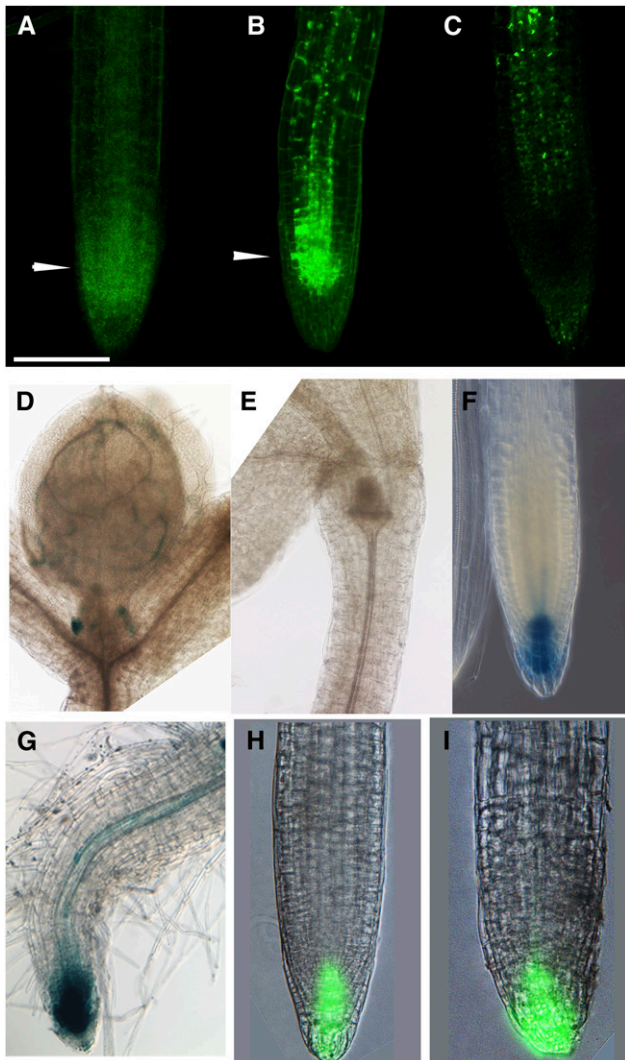


Figure 8. Auxin-Induced *APM1* Expression and Responsive Reporters in *apm1* Mutants.

- (A) to (C) *APM1* expression is auxin responsive.
 (A) Pro*APM1*:GFP signal is observed in 4-d-old root tip.
 (B) Pro*APM1*:GFP signal after 100 nM IAA treatment for 2 h is strongly enhanced in the stele but reduced in the epidermis. Arrowheads in (A) and (B) point to the region where the signal is observed in (A) but absent in (B). See Figure 9C for comparison following gravity stimulus.
 (C) Pro*APM1*:GFP signal after 1 μ M 2,4-D treatment for 2 h. A change seen in the subcellular pattern of the Pro*APM1*:GFP signal after 2,4-D treatment is an apparent result of altered reticulation of the endoplasmic reticulum after 2,4-D treatment.
 (D) to (I) Auxin accumulation in 5-d-old wild-type and *apm1* seedlings.
 (D) Pro*AA2*:GUS activity in control cotyledon.
 (E) Pro*AA2*:GUS activity is absent in *apm1-1* (+/–) cotyledon.
 (F) Pro*DR5*:GUS activity in 5-d-old control root.
 (G) Pro*DR5*:GUS activity in the *apm1-2* (+/–) root is greater than in the control.
 (H) Pro*DR5*:GFP signal in 5-d-old control root.
 (I) Pro*DR5*:GFP signal is greater in the 5-d-old *apm1-1* (+/–) root than in the control.
 Bars = 100 μ m in (A) to (C) and (F) to (I) and 200 μ m in (D) to (E).

established with ALTERED RESPONSE TO GRAVITY and the Rab GTPase family (Boonsirichai et al., 2003; Chow et al., 2008). Treatment with the fungal toxin BFA results in fusion of the *trans*-Golgi network with components of the endocytotic pathway/endomembrane system to form aggregates known as BFA bodies (Nebenführ et al., 2002; Tse et al., 2006). The size and shape of BFA bodies has been shown to be tissue specific (Robinson et al., 2008a; Pan et al., 2009). This effect is reversed when BFA is washed out of cells, and the fragmented endoplasmic reticulum, Golgi, and endomembrane system recover over time (Saint-Jore et al., 2002; Robinson et al., 2008b). When root tips were treated with 5 μ M BFA for 30 min, Pro*APM1*:YFP-APM1 signals were observed in large BFA bodies (see Supplemental Figure 7A to 7D online), and localization was restored 2 h after BFA washout (see Supplemental Figure 7E to 7G online). The size and number of BFA bodies that contain APM1 differ according to cell type, and some of those bodies are unlike those associated with aggregations of known endomembrane markers. It is also interesting to note that the BFA bodies in *apm1-1* transformed with Pro*APM1*:YFP-APM1 resemble those in the sterol mutant *fk-J709* transformed with Pro*PIN2*:PIN2-GFP (Pan et al., 2009).

PIN2 localization shows cell type-specific BFA or wortmannin sensitivity (Abas et al., 2006; Jaillais et al., 2006; Shin et al., 2005). Therefore, we examined the effect of wortmannin on APM1 localization and found that localization was altered in epidermal cells (see Supplemental Figure 7H to 7K online), the same cells where PIN2 localization is wortmannin sensitive (Jaillais et al., 2006). Like wortmannin, the limonoid prieurianin (recently marketed as endosidin) has been shown to affect PIN2, as well as AUX1 and BRI1 trafficking (Robert et al., 2008). However, treatment with 33 μ M endosidin had little effect on APM1 localization (data not shown).

In contrast with the ABCB integral membrane proteins isolated by NPA affinity chromatography whose activity is inhibited by NPA (Bernasconi et al., 1996; Murphy and Taiz, 1999a, 1999b; Murphy et al., 2000, 2002; Noh et al., 2001, 2003; Geisler et al., 2003, 2005; Terasaka et al., 2005), an NPA binding peripheral membrane protein from cucurbits appeared to be associated with the actin cytoskeleton (Cox and Muday, 1994; Butler et al., 1998). As APM1 is a peripheral membrane protein that binds both free and conjugated NPA (Murphy et al., 2000, 2002; Smith et al., 2003), we examined the cytoskeletal dependence of APM1 localization. Treatment with the actin depolymerizing agent latrunculin B resulted in intracellular agglomerations of APM1 signal, while the microtubule depolymerizing agent oryzalin had little effect (see Supplemental Figure 7L to 7S online), indicating that the subcellular localization of APM1 is primarily actin, rather than microtubule dependent.

APM1 and NPA

NPA is used as a pre-emergent herbicide for cucurbit crops that inhibits weed root growth and prevents seedling establishment. Resistance of crop plants to NPA appears to correlate with levels of NPA amidase activity (Makam et al., 2005), and APM1 was originally identified as the hydrolytic enzyme involved in NPA hydrolysis in planta (Murphy and Taiz, 1999a; Murphy et al.,

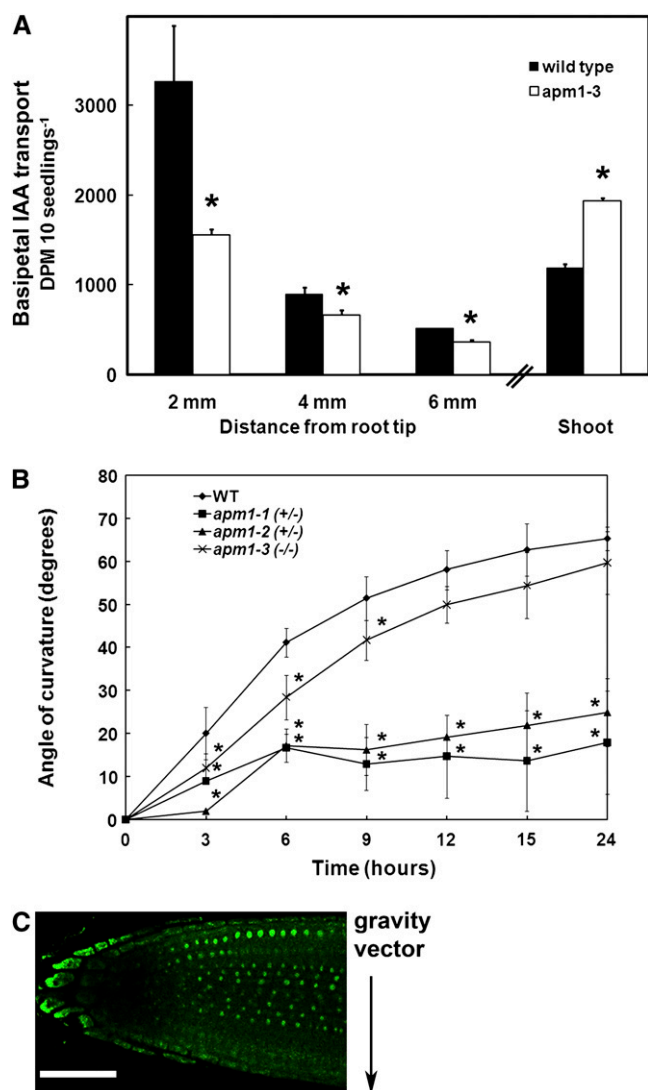


Figure 9. Auxin Transport and Gravitropism in *apm1* Mutants.

(A) Basipetal auxin transport is significantly reduced in the first 2 mm from the tip in *apm1-3* ($-/-$). This region coincides with the columella region, which exhibits the cell differentiation defects, and where the *DR5* reporter shows auxin accumulation. Basipetal auxin transport from the shoot apex of *apm1-3* ($-/-$) is enhanced compared with that of the wild type. Means and standard deviation from three independent experiments are shown (t test, $*P < 0.01$). It was not possible to reproducibly measure shoot basipetal auxin transport in 5-d-old *apm1-1* ($+/-$) or *apm1-2* ($+/-$) seedlings.

(B) Gravitropic response of *apm1-1* ($+/-$), *apm1-2* ($+/-$), and *apm1-3* ($-/-$) mutants compared with that of the wild type. Angle of curvature is reduced in the *apm1-1* and *apm1-2* mutant compared with the wild type. Means and standard deviation from two independent experiments are shown ($n = 50$; t test, $*P < 0.01$).

(C) ProAPM1:GFP signal is not observed on the auxin-accumulating side of the root after 30 min of gravity stimulus. Bar = 50 μm .

[See online article for color version of this figure.]

2000). This affinity for NPA was subsequently used to purify APM1 from *Arabidopsis* membranes, and recombinant APM1 was shown to bind free ^3H -NPA (Murphy et al., 2002). Low concentrations of NPA (0.1 to 5 μM) routinely used to alter auxin transport have no observable effects on membrane protein trafficking, but do phenocopy the elongation defects seen in *abc1 abc19* mutants (Murphy et al., 2000; Noh et al., 2001;

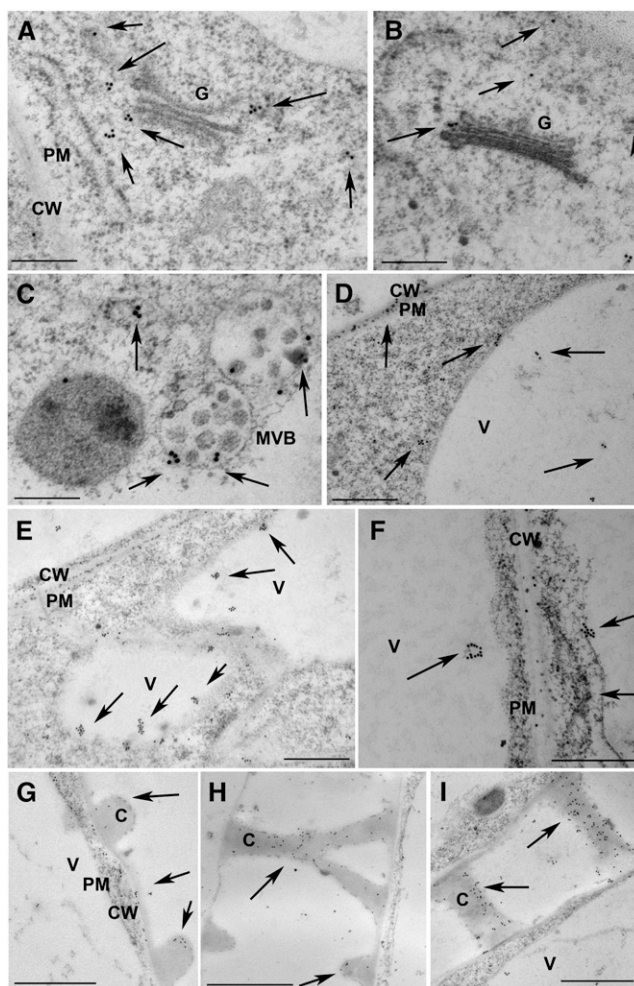


Figure 10. Analyses of APM1 Subcellular Localization by Electron Microscopy.

Immunogold localization of APM1 in high-pressure frozen/freeze-substituted 5-d-old seedlings. Arrows point to immunogold labeling of APM1. The experiment was repeated twice with each antibody. See Supplemental Figure 6 online for preimmune controls. Bars = in 500 nm in **(A)** to **(F)** and 1 μm in **(G)** to **(I)**.

(B) and **(D)** to **(G)** C terminus antibody.

(A), **(C)**, **(H)**, and **(I)** Peptide antibody.

(A) and **(B)** Labeling on Golgi stacks (G) and flanking cytoplasm in root cortical cells.

(C) Labeled multivesicular bodies (MVBs) in root cortical cells.

(D) to **(F)** Labeling on tonoplast, plasma membrane (PM), and cell walls (CW) of perivascular root cells. C, cytoplasm, V, vacuole.

(G) to **(I)** Labeling in metaxylem cells.

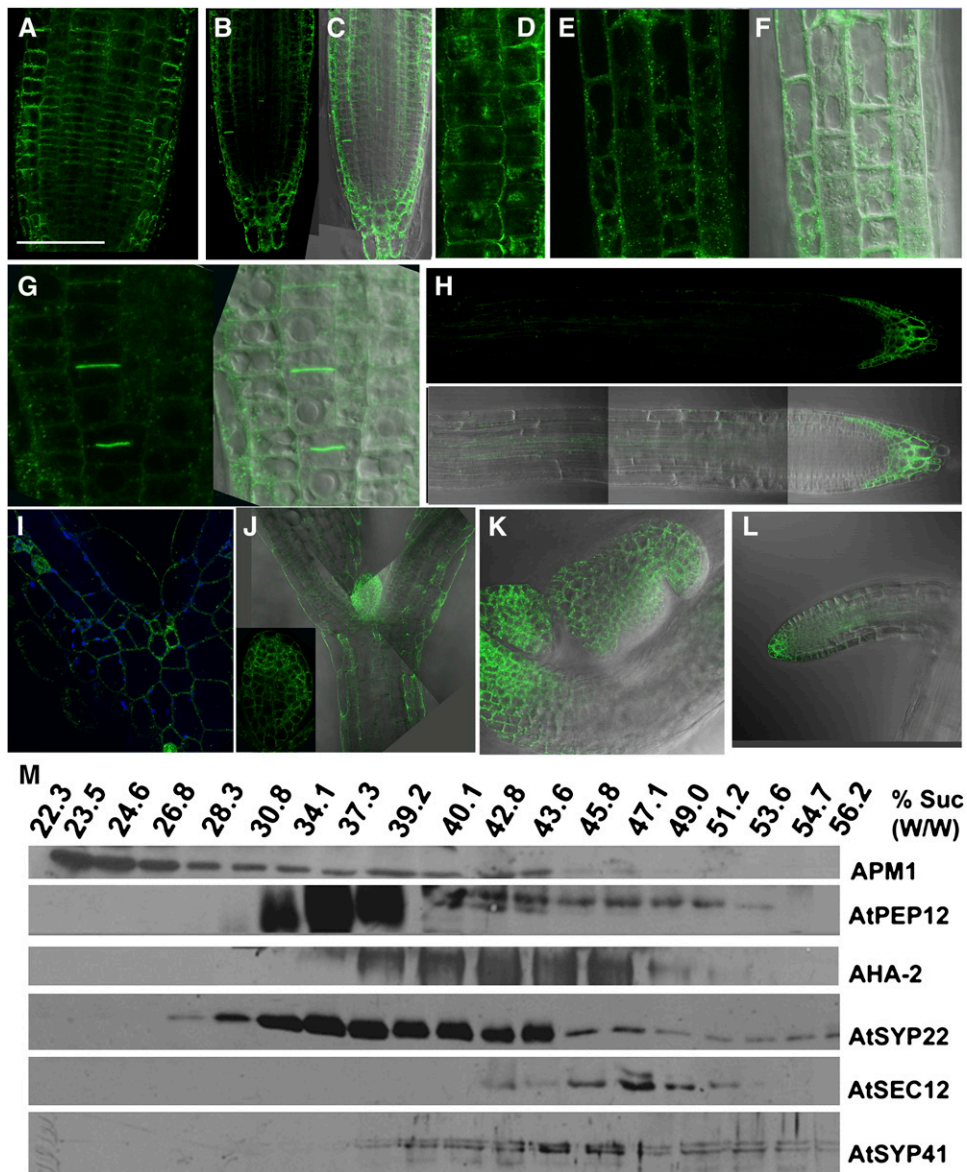


Figure 11. APM1 Subcellular Localization by Confocal Laser Scanning Microscopy and Colocalization with Compartmental Markers in Sucrose Density Gradients.

APM1 was immunolocalized using purified antisera generated against the C-terminal 30 kD of the protein (Murphy et al., 2002) or against a unique peptide (E₁₂₄-C₁₄₅) derived from the APM1 sequence adjacent to the hydrophobic membrane interaction domain (see Methods). The two antisera produced identical localization results. In addition, transformants were generated with ProAPM1:YFP-APM1 and ProAPM1:APM1-YFP constructs that complemented the *apm1-1* loss-of-function mutants (see Methods; Figures 4G and 4H; see Supplemental Figure 3 online). APM1 shows plasma membrane, endomembrane, and cytosolic localizations. Bars = 100 μ m in (A), (H), (J), and (K), 50 μ m in (B), (C), (G), and (I), 10 μ m in (D), and 20 μ m in (E) and (F).

(A) to (L) Subcellular localization of APM1 in 5-d-old seedlings using purified APM1 antisera ([A], [D], and [I]) and ProAPM1:YFP-APM1 ([B], [C], [E] to [H], and [J] to [L]).

(A) Immunolocalization of APM1 in root tips using the C terminus antibody.

(B) ProAPM1:YFP-APM1 in root tips.

(C) Differential interference contrast (DIC) overlay of (B).

(D) Immunolocalization of APM1 in root tips using the C terminus antibody showing subcellular localization.

(E) Subcellular localization of ProAPM1:YFP-APM1 in root tips.

(F) DIC overlay of (E).

(G) ProAPM1:YFP-APM1 localization at the newly forming cell plate (left) and DIC overlay (right).

(H) Localization of ProAPM1:YFP-APM1 in the root tip and metaxylem (top) and DIC overlay (bottom).

Table 2. Light Membrane Fraction Lipid Composition

Component	Relative Amount Light Membrane Fraction:Whole Microsomes
Neutral lipids	3.8 ± 0.3
Total sterols	2.1 ± 0.45
Glucosylceramide ^a	18% ± 1.6% total lipids (m/m)
C24 increase	33% ± 12%
C26 increase	28% ± 15%
Total phospholipids	<0.4

^aNot significant in whole microsomal membranes.

Partial determination of lipid composition of light membranes (24.6 to 28.3% sucrose) from sucrose density gradient fractionation of *Arabidopsis* microsomes. Composition analyzed via thin layer chromatography as by Lefevre et al. (2008) and gas chromatography/liquid chromatography–mass spectrometry as by Titapiwatanakun et al. (2009). Data are means ± SD, *n* = 3.

Geisler et al., 2003, 2005; Terasaka et al., 2005; Blakeslee et al., 2007). The *twd1* mutant shares many *abcb1 abcb19* phenotypes, and NPA has been shown to inhibit interactions between TWD1 and ABCB1/19 (Geisler et al., 2003; Bouchard et al., 2006; Bailly et al., 2008). However, even at higher concentrations, NPA treatment does not produce the twisting phenotype of *twd1*. Slightly higher concentrations of NPA have also been shown to phenocopy *pin* mutations, suggesting that PIN proteins are direct or indirect targets of NPA action (Stieger et al., 2002; Mravec et al., 2008). Saturating NPA concentrations (0.05 to 1 mM) have been shown to alter trafficking of the PIN1 auxin efflux carriers and other membrane proteins in *Arabidopsis* (Geldner et al., 2001, 2003, 2004; Dhonukshe et al., 2005, 2007; Kleine-Vehn et al., 2006). NPA inhibition of APM1 activity appears to be most evident when NPA is applied in concentrations between these two ranges (Murphy and Taiz, 1999a; Murphy et al., 2002).

Growth of wild-type seedlings on 30 μM NPA phenocopied the root phenotype of *apm1* mutants (Figures 12A to 12C), and cotyledonary defects are seen in *apm1* mutants observed when embryos develop in the presence of 10 μM NPA (Weijers et al., 2005); no additional phenotypes were observed when *apm1* was grown on 30 μM NPA (Figure 12D). A 2-h treatment with sufficient NPA (10 μM) to eliminate auxin transport from the shoot apex (Peer et al., 2004) increased ProAPM1:GFP expression in epi-

dermal and cortical cells within the lateral root cap and eliminated expression in the stele. After 30 min treatment with 30 μM NPA, ProAPM1:YFP-APM1 subcellular localization was not significantly altered compared with untreated root tips, but no APM1 signal was detected after 60 min of treatment (Figures 12E and 12F). However, treatment with 5 μM NPA did not affect APM1 signal. Some M1 APs function as dimers, and NPA may affect APM1 stability, as inclusion of NPA in buffers or affinity matrices increases the presence of a 42-kD APM1 fragment (Murphy et al., 2002).

Localization of Auxin Transporters in *apm1*

Since the *apm1-1* and *apm1-2* mutants exhibited altered auxin transport and gravitropism, the effect of *apm1* mutations on auxin transporters was examined. In the wild type, PIN1 localized to the bottom of cells in the stele and endodermis in immunohistochemical analysis (Figure 13A). In *apm1-1* roots, PIN1 signals in the root were reduced, but the polar membrane association was not affected (Figure 13B). In *apm1-2* roots, however, PIN1 was less abundant compared with in the wild type, and membrane association appeared diffuse (Figure 13C). We also examined PIN1-GFP localization in the *apm1-1* background. PIN1 signal was reduced and restricted to the center of the stele in *apm1-1*, but polar localization was still observed (Figures 13D and 13E). These alterations in PIN1 abundance and looser membrane association are similar to those seen in *Arabidopsis* transformants overexpressing the AVP1 H⁺-pyrophosphatase that exhibit enhanced apoplastic acidification and transport of shoot-derived auxin to the root (Li et al., 2005). They also resemble PIN1 abundance and localization in wild-type seedlings that have had IAA added to the shoot apex (Peer et al., 2004). In both cases, auxin transport to the root is increased, and altered PIN1 abundance is an indirect effect of increased auxin flux/accumulation.

In the wild type, PIN2 signals were on the top of epidermal cells and at the top and periclinal sides of cortical cells in the root tip in immunohistochemical analysis (Figure 13F), consistent with PIN2 function in transporting auxin away from the root tip and reflux to the quiescent center. In both *apm1-1* and *apm1-2*, the membrane association of PIN2 showed both association with the membrane and a diffuse signal (Figures 13G and 13H). We also examined PIN2-GFP localization in the *apm1-1* background.

Figure 11. (continued).

(I) Immunolocalization of APM1 in the shoot apical meristem using the C terminus antibody.

(J) ProAPM1:YFP-APM1 localization in the shoot apical meristem and epidermal cells of the hypocotyl. Inset: primary leaf.

(K) ProAPM1:YFP-APM1 localization in the shoot apical meristem of a 3-week-old plant.

(L) ProAPM1:YFP-APM1 localization in a lateral root of a 3-week-old plant. For these experiments, 50 seedlings were observed for immunolocalization studies, experiments were repeated five times, using both antibodies, and the C terminus antibody is shown here. Approximately fifty seedlings from each of seven YFP lines were examined. These localizations were observed in >90% of the individuals. Eight ProAPM1:APM1-YFP lines were also examined; however, YFP fluorescence was not observed, except in one line, which had a cytosolic signal.

(M) Protein gel blot analysis of sucrose density fractionation of *Arabidopsis* microsomal membranes probed with antisera to APM1, PEP12/SYP21, AHA-2, SYP22, SEC12, and SYP-41. The membranes were fractionated with a 14 to 55% continuous sucrose (w/w) gradient, and the sucrose concentration of each fraction was measured by its refractive index. A total of 25 μL of each fraction was loaded per lane. This experiment was repeated four times using both antibodies (two times each) with similar results. The representative western shown here was with the C terminus antibody.

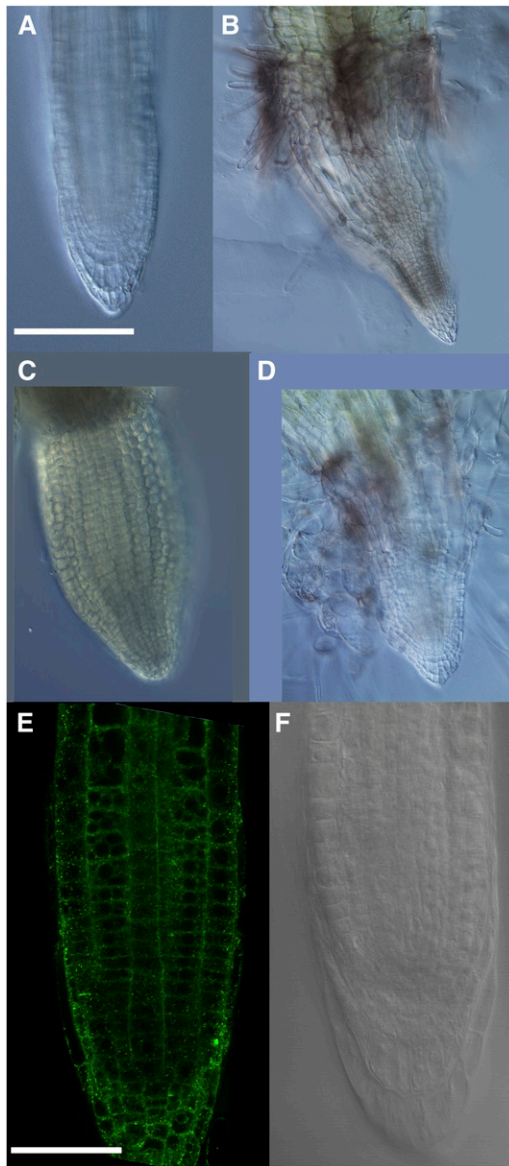


Figure 12. NPA Treatment Produces No Additional Root Phenotypes in *apm1-1* and Results in Loss of APM1 Signal.

- (A) Five-day-old wild-type root tip.
 (B) Wild type treated with a high concentration of NPA (30 μ M) can phenocopy *apm1* roots.
 (C) Five-day-old *apm1-1* (+/–) seedling showing abnormal primary root.
 (D) *apm1-1* (+/–) seedling grown on 30 μ M NPA.
 (E) ProAPM1:YFP-APM1 signal is observed after 30 min 30 μ M NPA treatment.
 (F) ProAPM1:YFP-APM1 signal is not observed after 60 min 30 μ M NPA treatment.
 Bars = 100 μ m in (A) to (D) and 50 μ m in (E) and (F).

PIN2 signal was reduced in *apm1-1*, but the signal was not sharply localized on the membrane and a diffuse signal was observed (Figures 13I and 13J). Since the root hair position in the trichoblasts of *apm1* was not different from those of the wild type, it appears that there is not a general defect in cell polarity. PIN2

mislocalization is consistent with APM1 localization in wild-type epidermal cells (Figure 11) and the alterations in gravitropism and auxin transport away from the root apex seen in *apm1* (Figure 9).

The auxin transport protein ABCB19/PGP19/MDR1 primarily transports auxin basipetally along the embryonic shoot to root axis and has a secondary role in remobilization of auxin within the lateral root cap (Geisler et al., 2005; Blakeslee et al., 2007; Lewis et al., 2007; Titapiwatanakun et al., 2009). In the wild type, ABCB19 is symmetrically localized in epidermal, cortical, endodermal, and mature vascular cells and localizes to the bottom of maturing vascular cells in the stele in immunohistochemical analysis (Figure 13K). In both *apm1-1* and *apm1-2*, ABCB19 localization from the membrane was partially disturbed (Figures 13L and 13M). We also examined ABCB19-GFP localization in the *apm1-1* background. ABCB19-GFP signal was more diffuse in the mutant background (Figures 13N and 13O). ABCB19 was initially copurified with APM1 from *Arabidopsis* microsomal membranes (Murphy et al., 2002). However, as ABCB19 polar localization appears to be linked to secondary cell wall formation (Blakeslee et al., 2007), altered ABCB19 localization in newly divided cells may be a result of the disordered growth seen in *apm1* roots. We also examined ProAUX1:AUX1-YFP localization in *apm1-1*. Although the AUX1 signal was reduced, the sub-cellular localization was not altered (data not shown).

FM4-64 Labeling and Uptake Are Altered in *apm1*

FM4-64 is a styryl dye commonly used to label the plasma membrane and monitor rates of endocytosis (Illinger and Kuhry, 1994; Betz et al., 1996; Ueda et al., 2001, 2004). Wild-type seedlings treated with FM4-64 show uptake of the dye within 15 min (Figure 13P). *apm1* mutants treated with the dye show altered staining of the plasma membrane (Figures 13Q to 13S). FM4-64-treated *apm1* seedlings were monitored over a 2-h time course and showed no increased plasma membrane labeling (all alleles) and little (*apm1-3*) or no uptake (*apm1-1* and *apm1-2*) of this dye (Figures 13Q to 13S). Therefore, plasma membrane labeling and trafficking of the styryl dye FM4-64 was altered in *apm1* alleles. This suggests that plasma membrane structure (sterol composition) and trafficking appear to be globally impacted in *apm1* mutants unlike that seen in *abcb19* mutants (Titapiwatanakun et al., 2009). This is also consistent with the altered PIN2 localization observed in *apm1* and the sterol dependence of PIN2 localization (Men et al., 2008).

DISCUSSION

APM1 Expression

Although APM1 is expressed ubiquitously throughout the plant during its life cycle, APM1 has three peaks in expression: during embryogenesis, in 3.5- to 5-d-old seedlings, and during senescence. During embryogenesis, APM1 is first expressed in the epidermis, then hypophysis, and then later in the vascular ground tissue. APM1 expression exhibits both early (within 30 min) and late (2 h) auxin responses, suggesting that this two-stage response may have different targets. In seedling roots, APM1 is

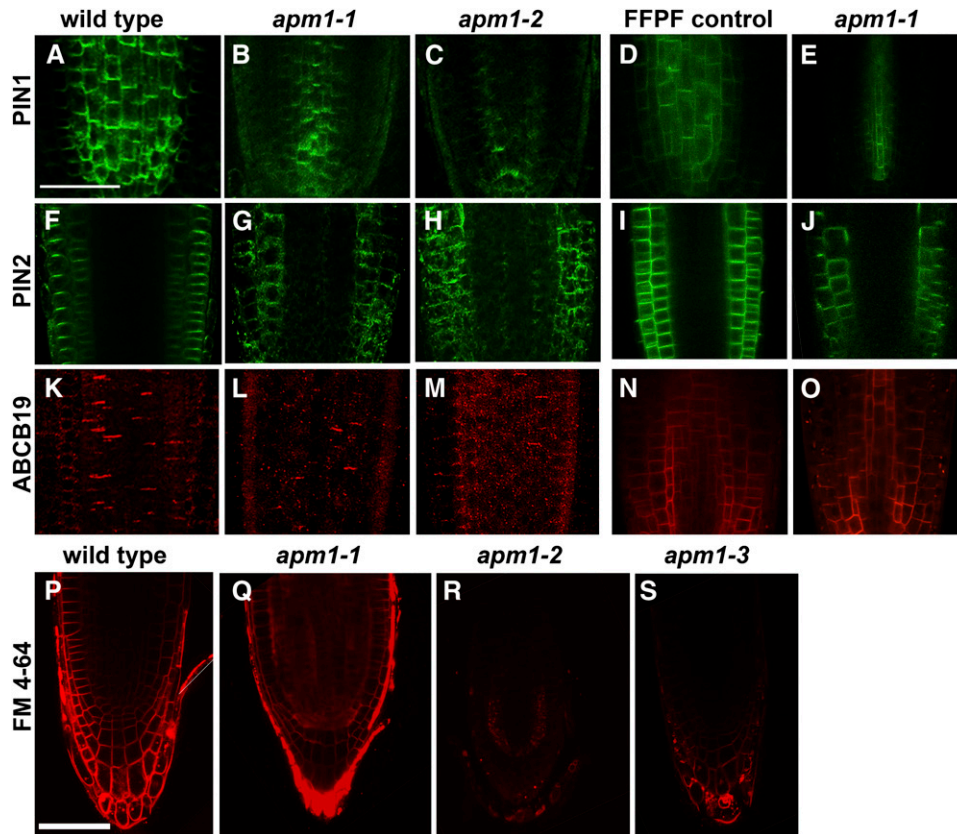


Figure 13. Localization of Auxin Transporters Are Altered in *APM1* Loss-of-Function Mutants.

(A) to (C) PIN1 immunolocalization.

(F) and (G) PIN2 immunolocalization.

(K) to (M) ABCB19 immunolocalization.

(D), (I), and (N) Functional fluorescent protein fusion controls in the respective mutant background.

(A) PIN1 immunolocalization signal in the wild type.

(B) PIN1 immunolocalization signal in *apm1-1* (+/-).

(C) PIN1 immunolocalization signal in *apm1-2* (+/-)

(D) PIN1-GFP signal in *pin1* transformed with ProPIN1:PIN1-GFP.

(E) PIN1-GFP signal in *apm1-1* (+/-). Restricted PIN1 subcellular and tissue-specific localization is consistent with altered auxin levels, an indirect effect of *apm1*.

(F) PIN2 immunolocalization in the wild type.

(G) PIN2 immunolocalization in *apm1-1* (+/-).

(H) PIN2 immunolocalization in *apm1-2* (+/-).

(I) PIN2-GFP signal in *eir1* transformed with ProPIN2:PIN1-GFP.

(J) PIN2-GFP signal in *apm1-1* (+/-). PIN2 localization is diffuse in *apm1* mutants.

(K) ABCB19 localization in the wild type.

(L) ABCB19 localization in *apm1-1* (+/-).

(M) ABCB19 localization *apm1-2* (+/-).

(N) ABCB19-GFP signal in *abcb19* transformed with ProABCB19:ABCB19-GFP.

(O) ABCB19-GFP signal in *apm1-1* (+/-). ABCB19 localization is diffuse in *apm1* mutants.

(P) to (S) FM4-64 signal in the wild type (P), *apm1-1* (+/-) (Q), *apm1-2* (+/-) (R), and *apm1-3* (-/-) (S).

Bars = 50 μ m.

[See online article for color version of this figure.]

expressed in the epidermis, and expression in the stele increases with auxin treatment, while expression in the epidermis decreases. Expression in the stele in 3.5- to 5-d-old seedlings corresponds to the maturation of the first protoxylem (3 d) and metaxylem elements (Busse and Evert, 1999a, 1999b). This

suggests that *APM1* may have roles in establishment or maintenance of ground tissue in both embryos and seedlings. *APM1* is also expressed in regions of organ transition, such as the root-shoot transition zone, shoot apical meristem, and in gynoecia and anthers, suggesting possible roles in modifying proteins that

are involved in specifying cell fate. Expression during early phases of xylem formation and during senescence may indicate a role for APM1 in programmed cell death.

APM1 Loss-of-Function Phenotypes

Root Meristem and Vasculature

APM1 appears to have two distinctive roles in root meristem and vascular tissue development and maintenance, one in embryogenesis and the other in seedling establishment. APM1 is required for normal cell division throughout embryogenesis and plays a role in the establishment of the hypophysis, the progenitor of the root meristem. This cell is not properly formed in loss-of-function mutants. During seedling development, APM1 is required for primary root meristem maintenance and identity. Severe *apm1* alleles ($-/-$) produce rootless seedlings. Seedling establishment does not occur because cell division in the root and shoot ceases (no *cyclinB1;1* expression in *apm1*), including in the quiescent center (little or no expression of quiescent center markers in *apm1*); therefore, the primary root does not continue to grow. Arrest in the G2/M phase can eventually induce apoptosis. PLETHORA (PLT) transcription factors are essential for specifying quiescent center stem cell identity and their position in the embryo and root (Aida et al., 2004; Galinha et al., 2007). *PLT1* and *PLT2* are expressed in the quiescent center in seedling roots, and *PLT3* and *BABY BOOM (BBM)* are expressed in the hypophysis and provasculature of the embryonic root (Galinha et al., 2007), as is *APM1*. We are exploring the hypothesis that PTL and BBM are targets of APM1 activity.

As a consequence of these meristematic defects, root architecture is affected. Cell files are not organized, and ground tissue identity is not properly established, as is exemplified by misexpression of *SCR* and *SHR*, transcription factors that regulate root patterning of the ground tissue and cell identity of the endodermis, in *apm1* (Figure 5). *SCR* is necessary for quiescent center identity and limits the *SHR* protein to the endodermis, where it is necessary for endodermis formation (Wysocka-Diller et al., 2000; Cui et al., 2007; reviewed in ten Hove and Heidstra, 2008). Whether this is a direct or indirect consequence of loss of APM1 activity remains to be addressed. It seems more likely that the altered expression of *SCR* and *SHR* may be due to the lack of a functional QC and subsequent cell identity specification, as two independent QC markers are not observed in *apm1*. APM1 does not exhibit a nuclear localization. Therefore, it is less likely that APM1 directly interacts with these transcription factors unless it is involved in cytosolic/membrane surface processing of these proteins or their interacting partners (Welch et al., 2007; Cui and Benfey, 2009).

MP is an auxin response factor (ARF5) transcription factor also involved in vascular patterning, and *APM1* and *MP* expression are coincident in the embryo, seedling root, and gynoecia (Hardtke and Berleth, 1998). Although, *apm1* does not exhibit the severe vascular patterning defects in the cotyledons and leaves observed in *mp*, the *mp* root phenotypes are similar to those of *apm1*. BDL is an auxin-induced IAA12 transcriptional repressor (Hamann et al., 2002) that interacts with MP to form the hypophysis (Hamann et al., 1999, 2002). Not surprisingly, *apm1*, *mp*, and *bdl* share similar root phenotypes. *APM1* expression

shows both primary and secondary responses to auxin induction. The possibility that MP and BDL are targets of APM1 activity or regulators of *APM1* auxin-responsive expression is being explored.

BXL1-1, a marker for protoxylem and xylem parenchyma cells, is also not expressed in *APM1* loss-of-function mutants (Figure 5). The absence of lateral roots in the mutants is also consistent with the improper formation of the vasculature. This again supports a role for APM1 in the development or maintenance of vascular tissue.

Embryo and Seedling Phenotypes

Aborted, arrested, and malformed embryos, which result in incomplete silique filling, are observed in siliques of *apm1* mutants (Figures 3 and 4). The transverse planes of cell division and arrested development observed in *apm1* embryos are also observed in *tomoz* embryos in *Arabidopsis* (Griffith et al., 2007); TOMOZ regulates mitotic exit and cytokinesis. Embryos that survive to maturity produce seedlings that often have fused and multiple cotyledons, resembling *GN* and quadruple *PIN* loss-of-function embryos and seedlings (Mayer et al., 1991, 1993; Friml et al., 2003). *apm1* and *gn* mutants also have similar seedling phenotypes, such as short roots, collapsed root meristems (15 d for *gn*), disorganized vasculature, absence of lateral roots, and agravitropism (Geldner et al., 2004). GN, an ADP-ribosylation factor G protein guanine-nucleotide exchange factor (Steinmann et al., 1999) that is a peripheral membrane protein with both cytosolic and membrane localization, functions in vesicle formation and secretion and shows BFA-sensitive localization when associated with membranes (Anders et al., 2008). Whether APM1 interacts with or is epistatic to GN remains to be addressed.

The *apm1* phenotypes, *APM1* expression data, and inducible silencing/expression results all indicate that APM1 has distinct roles during embryogenesis and seedling establishment (Figure 7). Embryonic abortion defects in *apm1* can be overcome by inducing *APM1* expression, and the incomplete silique filling and embryonic cotyledonary defects observed in *apm1* can also be induced by silencing *APM1* in wild-type plants.

Consistent with *APM1* expression patterns, ~3.5 d is the critical developmental time point that APM1 activity is required for normal root development to continue, as wild-type plants transformed with pOpOff show the arrested root phenotype after 3 or more days of silencing, and pOpOn transformed *apm1-1* show a longer root phenotype after 3 or more days of *APM1* induction. Importantly, seedling establishment is inhibited by *APM1* silencing in wild-type seedling with no embryonic defects (Figure 7). Therefore, APM1 activity has at least two distinct temporal roles, in embryogenesis and seedling establishment.

apm1 mutants appear to have cell adhesion defects in the hypocotyls and altered secretion of mucilage in germinating seeds, suggesting that *apm1* may have a defect in pectin secretion, as pectins are important components of cell wall adhesion (McCann et al., 1992) and mucilage (Western et al., 2000; Macquet et al., 2007). APM1 activity may be required for proper processing of the enzymes involved in biosynthesis of cell wall components. This is consistent with the cell adhesion defects observed in the hypocotyl but also indicates a role for

APM1 in the formation of metaxylem elements in the wild type. Alternatively, pectin fine structure is altered when auxin response factor *DR12* is downregulated in tomato (*Solanum lycopersicum*; Jones et al., 2002; Guillon et al., 2008), suggesting that the *apm1* cell adhesion defect is an indirect effect due to altered auxin transport in *apm1* and not a direct effect on pectin biosynthesis or secretion. We are currently investigating if pectin accumulations and depositions are altered in the *apm1* mutants. Although GN is most noted for its role in secretion of PIN1 to the plasma membrane (Geldner et al., 2003; Paciorek et al., 2005), GN functions in secretion of multiple cargo. For example, abnormal deposition and secretion of pectins is observed in *gn/emb30* (for *embryo defective 30*) (Shevell et al., 2000). The BFA-sensitive recycling of cell wall components, like pectins and xyloglucans, is important for root meristem maintenance and cytokinesis (Baluska et al., 2002, 2005). APM1 may function in cycling of cell wall components, as suggested by the electron-dense bodies associated with APM1 in electron micrograph results (Figure 10).

Mature Plants

Branched trichomes are observed in severe *apm1* alleles and rarely in the weak allele (Figure 6). Branched trichomes are usually a result of endoreduplication, and several classes of genes act as positive and negative regulators of trichome branching (Guimil and Dunand, 2007). Although the cell cycle is arrested in *apm1*, as *cyclinB1;1* expression is not observed in the root or shoot, ectopic expression of *cyclinB1;2* was shown to enhance trichome branching (Schnittger et al., 2002). Since *SCR* has ectopic expression in *apm1*, it may be that other genes are also ectopically expressed. APM1 appears to be associated with the cell plate, suggestive of a role in the cell cycle or recycling cell wall components.

In addition to peak APM1 expression during embryogenesis and in 3.5- to 5-d-old seedlings, the third time during *Arabidopsis* life cycle where *APM1* expression is high is in senescing leaves. The loss-of-function mutants show delayed senescence, pOpOn restored wild-type senescence to *apm1*, and overexpression of *APM1* enhanced progression through the life cycle. APM1 appears to have a role in metaxylem formation, as *APM1* is expressed and localized in the metaxylem, and the *apm1* mutants have disorganized vasculature. APM1 is also expressed in anthers. Xylem and anther maturation and senescence are all forms of terminal differentiation, a type of programmed cell death (reviewed in Beers, 1997). The roles of proteases in senescence has received recent attention (reviewed in Reape and McCabe, 2008), and APM1 could be involved in processing proteins for remobilization, turnover, or degradation.

APM1 in Auxin Responses and Non-Auxin Responses

A more direct role for APM1 with regard to auxin transport is indicated in the primary root, where *APM1* appears to regulate the basipetal redirection of auxin via PIN2 efflux carriers (Figures 9 and 13). This suggests that APM1 plays a positive role in regulating PIN2 function. By contrast, it appears that APM1 negatively regulates PIN1 and/or ABCB19 function, although this regulation appears to be indirect (Figure 9 and 13). The subcel-

lular localization of PIN1 and PGP19/ABCB19 is largely undisturbed in *apm1* heterozygotes, *APM1* expression increases in vascular tissue of auxin-treated roots, and shoot basipetal auxin transport increases in *apm1-3* (Figures 8, 9, and 13). Discrimination between interactions with PIN1 and ABCB19 has been complicated by the inability to recover homozygous double mutants from crosses of either *pin1* or *pgp19/abcb19* with *apm1*.

Some of the severe embryonic defects of *apm1* may be attributed to altered auxin transport and accumulation in the hypophysis. However, APM1 appears to negatively regulate basipetal auxin transport in the shoot, and PIN2, which exhibits altered localization in *apm1* mutants, plays no obvious role in embryonic development (Chen et al., 1998; Luschnig et al., 1998; Müller et al., 1998). As such, the embryonic defects seen in *apm1* mutants are less likely to be directly auxin dependent and are more likely to be related to mitosis and establishment of cell identity, since the hypophysis does not continue to develop. APM1 activity may depend on other developmentally important processes, as the defects observed in *apm1* mutants at the late globular stage coincide with Zn mobilization from the endosperm to the embryo (Otegui et al., 2002) and Zn is required for APM1 activity (Murphy et al., 2002).

High concentrations (5 to 50 μ M) of NPA produce multiple developmental changes in plants that are distinct from the growth responses seen when lower concentrations (0.1 to 3 μ M) of NPA are used to inhibit auxin transport (Okada et al., 1991; Garbers et al., 1996; Gälweiler et al., 1998; Marchant et al., 1999; Murphy et al., 2000, 2002; Petrásek et al., 2003; Dhonukshe et al., 2005). The extent to which NPA phenocopies *apm1* developmental, cellular, and biochemical phenotypes is consistent with direct inhibition of APM1 by NPA (Figures 3 and 12). Inhibition of the endocytosis of preprophase bands and subsequent alterations of planes of cell division by high concentrations of NPA (Dhonukshe et al., 2005) are also consistent with APM1 localization at the cell plate, suggesting a possible role in cell cycle check points. Cyclin Bs accumulate after the G2 checkpoint as the cell enters of mitosis (Colón-Carmona et al., 1999). The absence of *cyclinB1;1* expression in *apm1* (Figure 5) suggests that the cells are no longer undergoing mitosis, as is seen with treatments with high concentrations of NPA. However, a lack of APM1 localization in the nucleus and a lack of meiotic defects in *apm1* mutants (Figure 11, Table 1) excludes a direct role in mitosis as is the case with MPA1 in meiosis (Sanchez-Moran et al., 2004; Pradillo et al., 2007).

APM1 Activity Is More Analogous to Mammalian Puromycin-Sensitive Aminopeptidase Than Insulin-Responsive Aminopeptidase

M1 peptidases function within the cell and play essential roles in embryogenesis, reproduction, cell cycle progression, and cell viability (Brooks et al., 2003; Lyczak et al., 2006). APM1, aminopeptidase N (APN/CD13), and the puromycin-sensitive aminopeptidase (PSA) are all M1 APs with both cytosolic and membrane localization (Constam et al., 1995; de Gandarias et al., 1997; Murphy et al., 2002; Braccia et al., 2003). The closest human ortholog to APM1 is PSA, and APM1 is itself puromycin sensitive (Murphy et al., 2002). Puromycin treatment inhibits the

cell cycle at the G2/M phase, and PSA localization has both cytosolic and nuclear localization (Constam et al., 1995). PSA-deficient mice ($-/-$) produce less viable embryos, have reduced litter size, and are smaller and less fertile than the wild type, indicating that PSA is required for normal growth (Towne et al., 2008), while another PSA-deficient line was reported to be infertile (Osada et al., 2001a, 2001b). PSA is important in both generating and degrading MHC peptides, although this did not appear to have a bearing on viability of the PSA-deficient mice (Towne et al., 2008). In *Caenorhabditis elegans*, the PAM-1 PSA ortholog has been shown to be necessary for oocyte-to-embryo transition and establishment of anterior-posterior polarity and is necessary for cells to exit meiosis (Lyczak et al., 2006). APM1 metalloproteinase activity may be important for processing of proteins required for general cellular function (housekeeping), by either activating or deactivating proteins, including proteins involved in the cell cycle or in recycling cell wall components.

Membrane-anchored M1 proteins, such as the insulin-responsive aminopeptidase (IRAP), have been shown to process signaling peptides (Tsujimoto et al., 1992; Herbst et al., 1997; Albiston et al., 2004). Like IRAP, APM1 is found in a unique light membrane fraction not characterized by other markers (Figure 11). However, the lack of a transmembrane helix, extracellular enzymatic activity domain, and the unique N-terminal extension that mediates IRAP-GLUT4 interactions (Tsujimoto et al., 1992; Herbst et al., 1997; Albiston et al., 2004) indicates that APM1 does not process extracellular peptide hormones or mediate GLUT4-like trafficking. APN/CD13 functions in cell surface uptake of cholesterol and cell adhesion to the extracellular matrix (Kramer et al., 2005; Wulfaenger et al., 2008). APM1 localization at the plasma membrane suggests that it may have a role in processing proteins at the cytosolic side of this interface, as altered sterol labeling and cell adhesion are observed in the mutants.

APM1 is a single-copy gene, with haploinsufficiency seen in dominant-negative loss-of-function mutants with embryo- and seedling-lethal phenotypes. The dominant effects can be explained by dosage effects (*apm1-1*) and by the hypothesis that APM1 acts as a dimer in vivo, based on Tyr AP activity under reducing conditions and NPA inhibition of protein-protein interactions (Murphy et al., 2002). Therefore, in stoichiometric amounts, one good copy and one corrupted copy make a nonfunctional protein. Mammalian type II APs function as homodimers. APN dimerizes through noncovalent bonds (Luan and Xu, 2007), while APA and TRH-DE are linked by a single disulfide bond (Hesp and Hooper, 1997; Papadopoulos et al., 2000), although A-LAP is a monomer (Hattori et al., 2000). Deletion analysis showed that the C-terminal protein-protein interaction domain is required for proper localization and that proper localization is required for enzymatic activity of APA, indicating that the C terminus has chaperonin activity (Ofner and Hooper, 2002; Rozenfeld et al., 2004). Although *apm1-1* produces full-length wild-type APM1, the protein is present in small quantities, with a dosage insufficient to confer normal growth. *apm1-2* produces a truncated protein (APM1^{R667*}) that only contains the catalytic domain, while *apm1-3* has a point mutation (APM1^{A694V}) in the protein-protein interaction domain. Therefore, APM1-APM1, APM1-APM1^{R667*}, and APM1^{R667*}-APM1^{R667*} may form in

apm1-2 heterozygotes, with two-thirds of the total protein being nonfunctional and producing a severe phenotype, consistent with a lack of full complementation, while *apm1-3* only has APM1^{A694V}-APM1^{A694V} and the phenotype is weak and can be complemented. The dimerization and roles of the catalytic and protein-protein interaction domains and potential targets of APM1 activity identified in the proteomics and in yeast two-hybrid analyses are currently under investigation.

METHODS

Gene Expression Analysis

RNA was extracted with the RNeasy Kit (Qiagen) from 5-d-old seedlings. cDNA was prepared from total RNA with Bioscript Reverse Transcriptase (BioLigne). Transcript levels were determined on a Bio-Rad iCycler IQ using iQ Sybr Green Supermix (Bio-Rad) in 20- μ L reactions. An aliquot of the RT reaction was used as template. PCR conditions were as follows: 1.5 min at 95°C (one cycle); and 30 s at 95°C, 30 s at 54°C, and 30 s at 72°C (35 cycles). Gene-specific primers used were as follows: 5'-TTTTGGCTGATAGGAACACT-3' and 5'-GTGAAGTAGCTTGGAAATGG-3'. Each RT sample was assayed in triplicate. Data were further analyzed in Excel. Transcript levels were normalized to tubulin 6 (primers 5'-TGG-GAACTCTGCTCATATCT-3' and 5'-CAGTGAAACCTCATTCTTTG-3').

Promoter:Reporter Constructs

To generate the Pro*APM1*:GFP construct, a 500-bp region of genomic DNA was PCR amplified using the following primers: 5'-region, 5'-CGGGGTACCTGATGAAGCTACGT-3'; 3' region, 5'-CGGAACTG-CAGTTTCTATTACTTGCAGAT-3'. The PCR fragment was inserted in the *Pst*I and *Kpn*I sites of the pGreen-GFP plasmid. To generate the Pro*APM1*:GUS construct, pGreen Luciferase was digested with *Not*I and *Sma*I to remove the Luciferase gene. The GUS gene was PCR amplified with the *Not*I and *Sma*I sites and introduced into the plasmid. For Pro*APM1*:GFP, 11 transgenic lines were obtained on kanamycin plates, of which nine showed similar expression patterns. These nine lines were used for all the studies. Five Pro*APM1*:GUS transgenic seedlings were obtained with similar expression patterns. The expression pattern of GUS and GFP was identical, indicating that they reflected correct *APM1* expression and had no insertional errors, which was also verified by sequencing. The GFP lines showed similar expression tissue-specific patterns, including a line that showed nuclear envelope localization (shown in Figures 2N to 2R), which was used in seedling roots because it shows the results more clearly in seedling roots than the other lines. Although we did not clone and sequence the insertion for this line, we surmise that a nuclear localization signal from *Agrobacterium tumefaciens* was inserted into the sequence during transformation or subsequent rearrangement.

Protein-Reporter Fusion Constructs

To construct Pro*APM1*:YFP-APM1, the primers 5'-CGGGATC-CATGGCCTCCTCCGAGGACG-3' and 5'-CGGAATTCTCCGACTTG-TACAGCTCGTCCATGCCGAGA-3' were used to amplify the YFP gene lacking a stop codon. The resulting PCR fragment was inserted into *Bam*HI and *Eco*RI sites of the cassette containing the *APM1* promoter inserted as above. *APM1* cDNA was PCR amplified using the following primers: primer 5'-CGGAATTCATGGATCAGTCAAAGGTG-3' and 5'-CGGAATTCGGTTAGTTTGAAGAGAGC-3'. Pro*APM1*:APM1-YFP was generated in a similar way, except that the *APM1* cDNA was inserted at the *Bam*HI and *Eco*RI sites before the YFP containing a stop codon. The

entire fragment was cloned into pGreen 0029 to generate the binary vector. *apm1-1* (+/-) and *apm1-2* (+/-) plants were transformed by the floral dipping method (Clough and Bent, 1998) and selected on kanamycin plates or by spraying Basta. Eight lines of ProAPM1:YFP-APM1 were obtained, of which eight showed YFP signal, all with similar tissue-specific and subcellular localization patterns. Eight lines of ProAPM1:APM1-YFP lines were obtained, one of which showed a cytosolic YFP signal. All the transgenic analyses studies were performed with T2 progenies. Twenty Pro35:YFP-APM1 and 15 Pro35S:APM1-YFP lines were obtained. The Pro35:YFP-APM1 lines showed the same localization patterns as the native promoter but had more puncta. The lines complemented the mutants, except that the plants progressed through the life cycle more quickly than the wild type. No Pro35S:APM1-YFP lines showed a signal, and all protein fusion constructs complemented the mutant phenotype, with the exception of *apm1-2*, which was not fully complemented. ProAPM1:APM1-YFP (and Pro35S:APM1-YFP; data not shown) C-terminal fusion transformants in the *apm1-1* background showed no signal (except one ProAPM1:APM1-YFP line showed cytosolic signal), even though the constructs complemented the *apm1-1* mutant phenotypes; Figures 4G and 4H); subsequent protein gel blot analysis with anti-YFP revealed that the YFP was cleaved from the fusions (see Supplemental Figure 8 online).

Inducible Constructs for Silencing and Expression of APM1

A suitable fragment from APM1 cDNA was identified and amplified by PCR using the primers (5'-CACCTGGAGCAGATGCAAATCAAG-3') and (5'-TCCCAACTTACACCGGAAAG-3') and then subcloned into pENTR-D/TOPO and subsequently into the Gateway binary vector pOpOff2. Cloning using gateway vectors was done using reagents and protocols from Invitrogen. The above procedure was used for generating constructs using pOpOn 2.1 vector Gateway binary vector using the primers (5'-CACCATGGATCAGTTCAAAGGTGAGCCT-3') and (5'-TTAGTTGAGAGAGCTGAGCAACG-3') to amplify full-length APM1, with either a YFP tag fused at the N-terminal portion of the gene or an HA tag. Constructs were introduced into *A. tumefaciens* C58 pGV3850 by electroporation. Col-0 plants were transformed with the pOpOff construct, and *apm1-1* (+/-) plants were transformed with the pOpOn construct by the floral dip method (Clough and Bent, 1998). Five independent lines of each pOpOff and pOpOn were examined, showing identical results. Resulting transformants were selected on Murashige and Skoog (MS) plates supplemented with kanamycin (50 mg mL⁻¹) and genotyped. Dex was dissolved in either DMSO or ethanol and kept as a 20 mM stock at -20°C. Unless otherwise stated, 10 μM Dex was used. Dex was added to quarter-strength MS media (pH 5.5, 1% agar) to achieve induction during seed germination or after seedling transfer in sterile conditions. For application to soil-grown plants, transgenic plants carrying the inducible construct were subjected to varying concentrations of DEX (0 to 10 μM) every 3 d.

Loss-of-Function Mutants

Initially, EMS and T-DNA insertion lines containing mutations in the APM1 gene (promoter, intron, and exon) from public collections were identified and analyzed but were found to exhibit wild-type levels of APM1 gene expression and/or conservative nucleotide substitutions. APM1 loss-of-function mutants were finally obtained from EMS mutagenesis of the catalytic region (Till et al., 2003), reasoning that the mutation must be embryo lethal and a point mutation may survive. Subsequently, a T-DNA insertion in the promoter region was identified (Alonso et al., 2003) and is analyzed here. *apm1-1* plants were genotyped as follows: PCR with Lba1 primer 5'-TGGTTCACGTAGTGGCCATCG-3' and 5'-TGATGAAGC-TACGTCCAACATGGCGG-3' were used to determine if the transformant contained a T-DNA mutation. To determine if the seedling was homozy-

gous for the T-DNA mutation, PCR was performed with primers 5'-TGATGAAGCTACGTCCAACATGGCGG-3' and 5'-CTTTTATAATAC-GAGGGTTGTAAGC-3'. To determine if the transformant contained the point mutation (*apm1-2* or *apm1-3*), an amplicon was generated using gene-specific primers (5'-TTCATTGGCGTTTTCCAGTTTGCTG-3' and 5'-TTACACCGGAAAGTCCATAAAGTC-3'), and the amplicon was digested with *XmnI* for *apm1-2*, which is lost in *apm1-2*, or *AluI* for *apm1-3*, which is gained in the *apm1-3* mutant.

Growth Conditions

Seedlings were grown on 1% phytagar plates, containing quarter-strength MS basal salts, pH 5.5, at 22°C, 14 h at 100 μmol m⁻² s⁻¹ except as indicated for specific treatments. *apm1* mutants were transferred to 1% phytagar plates containing quarter-strength MS basal salts, pH 5.5, supplemented with 1% sucrose at 24°C to induce adventitious root formation from the hypocotyls prior to transfer to soil; however, a robust root system never formed. The higher growth temperature was used to enhance auxin production (Gray et al., 2003). Plants on soil were grown in the greenhouse under natural light conditions, and in the winter, the daylength was extended to 16 h with HID lights (150 μmol m⁻² s⁻¹). See <http://www.hort.purdue.edu/hort/facilities/greenhouse/hlaTech.shtml> for more information. Inflorescence phenotypes of *apm1* alleles varied under the different light conditions.

APM1 Peptide Antibody

Antisera were generated in two rabbits against the peptide acetyl-EHNGEKKNMAVTQFEPADARRC-amide, which was derived from the sequence (E₁₂₄-C₁₄₅) in APM1 immediately adjacent (C-terminal) to the hydrophobic interaction domain by Cambridge Research Biochemicals. The antiserum was initially purified against the peptide but exhibited such high affinity to the peptide that it had to be eluted by unacceptably extreme changes in salt or pH. The antisera were instead purified against ProteinA. An antibody previously generated to the C terminus of APM1 (Murphy et al., 2002) was also used.

Immunohistochemical Localization and Immunofluorescence Studies

Arabidopsis thaliana seedlings (wild type Col-0, *apm1-1*, and *apm1-2*) were grown on 1% phytagar plates, containing quarter-strength MS basal salts, pH 5.5, 22°C, and 14 h, at 100 μmol m⁻² s⁻¹, and 5-d seedlings were prepared for immunolocalization as follows: seedlings were fixed in 4% *p*-formaldehyde in microtubule stabilizing buffer (MTSB) solution (50 mM PIPES, 5 mM EGTA, and 5 mM MgSO₄) and 5% DMSO for 1 h. They were washed with MTSB + 0.1% Nonidet P-40 for 10 min (five times), and this was followed by 10-min washes (five times) in distilled water. The seedlings were then digested with 0.5% Pectolyase (Seishin) and 0.1% macerozyme (cellulose in some cases) for 30 min at 37°C for another 30 min at room temperature. They were washed in MTSB and distilled water (five times each). Digested seedlings were permeabilized for 1 h in 10% DMSO and 1% Nonidet P-40 and then blocked with 3% BSA in MTSB for 1 h. Seedlings were incubated overnight (37°C) with anti-APM1 (1:500), anti-PIN1 (1:400), or anti-PIN2 (1:250) antibodies in 3% BSA in MTSB. They were washed for 10 min (six times) in 0.1% Triton X-100 and then for 10 min (three times) in MSTB and then incubated for 3 h at 37°C in goat anti-rabbit-Alexafluor 488 (1:250) or anti-rabbit-Cy3 (1:600) in 3% BSA/MTSB. They were washed in MTSB/0.1% Triton X-100 and then in water for 10 min each (five times).

Immunofluorescence analysis was performed using a Bio-Rad 2100 confocal laser scanning microscope equipped with argon (488 nm) and He-Ne (543 nm) lasers or a Carl Zeiss LSM510-META or LSM 710 confocal laser scanning microscope. The following settings were used for

AlexaFluor488 and GFP: 488-nm argon laser power 5%, the pinhole was at 1 Airy Unit (38 μm), the 488-nm filter, gain 30 to 50 (Bio Rad) or 603 (Zeiss). For YFP: 514-nm argon laser power 10% (LSM510) or 5% (LSM710), the pinhole was at 1 AU (38 μm), the 458 nm/514 nm dichroic, emission 520 to 550 nm in ChS1, gain 550 (LSM510) or 603 (LSM710), pixel dwell time 25.6 μs . For propidium iodide and FM4-64 (*N*-(3-triethylammoniumpropyl)-4-(*p*-diethylaminophenyl)-hexatrienyl) pyridinium dibromide): 594-nm laser 5%, the pinhole was at 1 AU (38 μm), the 488/594 filter, gain 700 (LSM510) or 603 (LSM710). Zeiss objectives used were C-Apochromat $\times 40/1.20$ W correction UV-VIS-IR M27 and C-Apochromat $\times 63/1.20$ W correction UV-VIS-IR M27. Expression analyses and subcellular localization studies with GFP and YFP reporter lines were performed with 3- to 5-d-old seedlings grown in continuous light. For expression analyses in embryos, siliques at different stages of development were collected from Pro*APM1*:GFP plants and the embryos were dissected out from the seed coat under a dissecting scope. The embryos were mounted on water and imaged with the confocal microscope. Epifluorescence, brightfield and DIC images were taken with a Nikon Eclipse 800, mercury arc lamp, ex 488, BA 515-530.

GUS Analyses

Three- to four-day-old seedlings were incubated in staining buffer (0.1 M NaPO₄, pH 7.0, 10 mM EDTA, 0.5 mM K ferrocyanide, and 0.1% Triton X-100) containing 50 to 100 mg X-gluc per 100 mL. *apm1-2* heterozygote mutants were crossed to plants transformed with the Pro*DR5*:GUS auxin reporter gene. The *apm1-1* mutants were also crossed to Pro*IAA2*:GUS and Pro*DR5*:GFP auxin-responsive reporters. Lines homozygous for the reporter were selected on kanamycin plates, and then PCR amplification followed by restriction digestion analyses was used to select the heterozygous mutant line. The seedlings were stained in the above solution 2 h at 37°C, and seedlings homozygous for the mutation were selected by their phenotypes and imaged.

Electron Microscopy

Electron microscopy was performed using the two APM1 antibodies and preimmune antisera, as outlined by Otegui et al. (2002).

Inhibitor Treatments

For inhibitor studies, wild-type and *apm1-1* (+/−) seeds were germinated on 1% phytagar plates with 30 μM NPA. Five-day-old seedlings were imaged with a Nikon E800 microscope. Five-day-old wild-type and Pro*APM1*:YFP-APM1 seedlings were incubated in 5 μM propidium iodide (15 min), 1 μM or 5 μM NPA (1 h), 5 μM BFA (30 min), 33 μM wortmannin (1 h), 10 μM latrunculin B (1 h), or 10 μM oryzalin (1 h) in an eppendorf tube, washed, and imaged using Zeiss LSM 510. Five-day-old seedlings were stained in 5 μM FM4-64 for 5 min (wild type) up to 2 h (*apm1* alleles) prior to confocal imaging on a Zeiss LSM 710. Reagents were from Sigma-Aldrich.

Whole-Mount Embryo Studies

Siliques at different stages of development were fixed in acetic acid and ethanol 1:9 for an hour and then treated with chloral hydrate:glycerol: water (8:1:2) overnight at room temperature. Specimens were mounted on chloral hydrate and observed under the microscope for heart-shaped embryos. The method described by Truernit et al. (2008) was used for the remaining embryo study.

Sucrose Gradient Fractionation and Protein Gel Blots

Arabidopsis seedlings (50 g) were homogenized in three volumes of 25 mM HEPES KOH, pH 8.5, 20 mM EDTA, 3 mM DTT, 290 mM sucrose, and

1 mM PMSF using a mortar and pestle. The homogenate was centrifuged at 8000g for 15 min to remove the debris, and the microsomal membrane fraction was pelleted by ultracentrifugation at 100,000g for 50 min. The pellet was resuspended in 3 mL of gradient buffer (10 mM Tris-MES, pH 7.0, 1 mM DTT, 250 mM sucrose, and 1mM PMSF) and centrifuged at 100,000g for 12 h on a 10-mL continuous gradient of 14 to 55% (w/w) sucrose in MIB with a 0.5 mL 60% (w/w) sucrose cushion. Fractions (0.5 mL) were carefully collected and stored at -80°C until further analyses. The density of each fraction was determined by a refractometer. For protein gel blots, anti-APM1 antibody was used at 1:500, AHA-2 at 1:2000, Syp22 at 1:1000, Sec12 at 1:2000, Syp41 at 1:500, and Pep12 at 1:2000 dilutions. Horseradish peroxidase-conjugated goat anti-mouse IgG and goat anti-rabbit IgG antibodies were used at a dilution of 1:10,000.

Five-day-old *Arabidopsis* seedlings (1 g) were homogenized in 2.5 mL homogenization buffer (0.29 M sucrose, 25 mM HEPES, pH 8.5, 20 mM EDTA, 0.5% PVP, 3 mM DTT, and 20 $\mu\text{g}/\text{mL}$ complete protease inhibitor cocktail [Sigma-Aldrich] and centrifuged at 8000g for 5 min at 4°C to obtain microsomal membranes. Then, 0.5 mL of supernatant was centrifuged at 100,000g for 1 h at 4°C. Pellets were resuspended in homogenization buffer or 0.1 M Na₂CO₃, pH 11.5, and 1% Triton X-100 or 1% SDS. The resuspended pellets were centrifuged at 100,000g for 1 h at 4°C. Samples were run on an 8% SDS-PAGE gel, followed by protein gel blot analysis using anti-APM1 (1:2000 in 5% skim milk in TBS and 0.1% Tween 20, 16 h, 4°C) followed by incubation with the secondary antibody (1:5000, 3 h, 4°C) and incubation with ECL (Pierce) for 5 min. AHA2 and APP1 antisera were as previously described (Murphy et al., 2002; Titapiwatanakun et al., 2009).

Gravitropism Assay

For analyzing the expression pattern of *APM1* in response to a gravity stimulus, 5-d-old Pro*APM1*:GFP seedlings were gravistimulated by rotating the plate by 90° for 30 min. To analyze the response of *apm1* mutants to a gravity stimulus, *apm1* seedlings were grown on half-strength MS media with 1% (w/v) phytoagar, pH 5.2, for 4 d. Plates were kept in a vertical position. After reorienting the plates by 90°, the root tip position was marked every 3 h over a 24-h time period. The angles of curvature were measured using the Image J program, and the data were analyzed by Microsoft Excel. Averages and standard deviations were calculated from 50 seedlings.

Auxin Transport Assay

Basipetal root and shoot auxin transport assays were performed as previously described (Geisler et al., 2005). Briefly, for root assays, *Arabidopsis* seedlings were grown on half-strength MS media under constant light for 4.5 to 5 d after germination. Before performing the assay, 10 seedlings were transferred to vertically discontinuous filter paper strips saturated in one-quarter MS and allowed to equilibrate for 2 h under yellow light. Auxin solutions used to measure transport were made up in 0.25% (w/v) agarose containing 2% (v/v) DMSO and 25 mM MES, pH 5.2. Under yellow light, a 0.1- μL microdroplet containing 500 nM unlabeled IAA and 500 nM [³H]IAA (specific activity 25 Ci/mmol; American Radiochemicals) was placed on the root tip of seedlings using a microliter Hamilton syringe. Seedlings were then incubated in yellow light for 5 h. After incubation, the root tips were removed. Three 2-mm sections of filter paper with 2-mm segment of tissue containing the 2 to 4 mm, 4 to 6 mm, and 6 to 8 mm from root tip were harvested separately. Additionally, a 4-mm filter paper strip section containing the remaining part of the seedlings was also harvested. Five milliliters of EcoLite scintillation fluid was added to each vial, and the vials were vortexed for 10 s and incubated for 48 h. The vials were vortexed 10 s again, and DPM was measured in a scintillation counter. For shoot assays, radiolabeled IAA was deposited at the shoot apex instead of the root tip columella, and the seedlings were cut with a razor blade. The

radioactivity of the cotyledons and upper hypocotyls was counted separately from the 2-mm paper strip with the root-shoot transition zone. See <http://www.hort.purdue.edu/hort/research/murphy/The%20more%20than%20complete%20hitchhiker%27s%20guide%20to%20auxin%20transport.pdf> for the complete protocol.

Materials from Other Laboratories

QC-25 and QC-104 markers were kind gifts from Ben Scheres (Bechtold et al., 1993). *SCR* and *SHR* constructs were kind gifts from Phil Benfey (Wysocka-Diller et al., 2000). *CyclinB1;1pro*:GUS was a kind gift from Peter Doerner (Colón-Carmona et al., 1999). *BXL1-1pro*:GUS was previously described (Goujon et al., 2003). *DR5pro*:GUS was a kind gift from Tom Guilfoyle (Ulmasov et al., 1997). *DR5pro*:GFP was a kind gift from Jiri Friml (Friml et al., 2003). *IAA2pro*:GUS was a kind gift from Ranjan Swarup (Swarup et al., 2001). *PIN1pro*:PIN1-GFP was a kind gift from Jiri Friml (Benková et al., 2003). *PIN2pro*:PIN2-GFP was a kind gift from Christian Luschnig (Abas et al., 2006). *ABCB19pro*:ABCB19-GFP was previously described (Blakeslee et al., 2007).

Accession Numbers

Sequence data from this article can be found in the Arabidopsis Genome Initiative or GenBank/EMBL databases under the following accession numbers: *APM1* (At4g33090), *PIN1* (At1g73590), *PIN2* (At5g57090), *ABCB19* (At3g28860), *AHA2* (At4g30190), *Syp22* (At5g46860), *Sec12* (NC_001146), *Syp41* (At5g26980), *Pep12* (NM_001021007), *APP1* (At4g36760), *AHA2* (At4g30190), *cyclinB1* (At4g37490), β -xylosidase (*BXL*) (At5g49360), *SCR* (At3g54220), *SHR* (At4g37650), and *AUX1* (At2g38120).

Supplemental Data

The following materials are available in the online version of this article.

Supplemental Figure 1. Microarray Data from Genvestigator and *Arabidopsis* eFP.

Supplemental Figure 2. Controls for Autofluorescence, Immunolocalization, Protein Gel Blots, and Analysis of APM1 Topology.

Supplemental Figure 3. Additional Images of Mutant Phenotypes and Complemented Mutants.

Supplemental Figure 4. Quantitative Real-Time PCR Analysis of Inducible Silencing and Induction of *APM1* Expression and Quantitation of Seed Data.

Supplemental Figure 5. Quantitative Real-Time PCR Analysis of Two-Stage *APM1* Expression after IAA Treatment.

Supplemental Figure 6. Electron Micrograph of Preimmune Controls.

Supplemental Figure 7. Trafficking Inhibitors Alter APM1 Localization.

Supplemental Figure 8. Leaf Phenotypes, Protein Gel Blot of YFP C-Terminal Fusions, Additional 35S Overexpression Data, and *SCR* Expression in *apm1-1* (–/–).

ACKNOWLEDGMENTS

This work was supported by the USDA (Grant 2002-01377), the National Science Foundation (0521881), and Biotechnology and Biological Science Research Council Underwood fellowship to A.S.M. and NSF-MCB-0619736 funding to M.S.O. We thank Ian Moore for discussions and his invaluable expertise and assistance with confocal laser scanning microscopy imaging. We thank the Arabidopsis TILLING project, espe-

cially Brad Till, as *APM1* was one of the initial pilot genes. We thank Brian Dilkes for discussions and suggesting the format for Table 1. We thank the ABRC. We thank all the reviewers for their helpful comments that have improved the manuscript.

Received March 24, 2008; revised May 14, 2009; accepted June 1, 2009; published June 16, 2009.

REFERENCES

- Abas, L., Benjamins, R., Malenica, N., Paciorek, T., Wisniewska, J., Moulinier-Anzola, J.C., Sieberer, T., Friml, J., and Luschnig, C. (2006). Intracellular trafficking and proteolysis of the Arabidopsis auxin-efflux facilitator PIN2 are involved in root gravitropism. *Nat. Cell Biol.* **8**: 249–256.
- Aida, M., Beis, D., Heidstra, R., Willemsen, V., Bilou, I., Galinha, C., Nussaume, L., Noh, Y.S., Amasino, R., and Scheres, B. (2004). The PLETHORA genes mediate patterning of the Arabidopsis root stem cell niche. *Cell* **119**: 109–120.
- Albiston, A.L., Ye, S., and Chai, S.Y. (2004). Membrane bound members of the M1 family: More than aminopeptidases. *Protein Pept. Lett.* **11**: 491–500.
- Alonso, J.M., et al. (2003). Genome-wide insertional mutagenesis of *Arabidopsis thaliana*. *Science* **301**: 653–657.
- Anders, N., Nielsen, M., Keicher, J., Stierhof, Y.D., Furutani, M., Tasaka, M., Skriver, K., and Jürgens, G. (2008). Membrane association of the *Arabidopsis* ARF exchange factor GNOM involves interaction of conserved domains. *Plant Cell* **20**: 142–151.
- Bailly, A., Sovero, V., Vincenzetti, V., Santelia, D., Bartnik, D., Koenig, B.W., Mancuso, S., Martinoia, E., and Geisler, M. (2008). Modulation of P-glycoproteins by auxin transport inhibitors is mediated by interaction with immunophilins. *J. Biol. Chem.* **283**: 21817–21826.
- Baluska, F., Hlavacka, A., Samaj, J., Palme, K., Robinson, D.G., Matoh, T., McCurdy, D.W., Menzel, D., and Volkmann, D. (2002). F-actin-dependent endocytosis of cell wall pectins in meristematic root cells. Insights from brefeldin A-induced compartments. *Plant Physiol.* **130**: 422–431.
- Baluska, F., Liners, F., Hlavacka, A., Schlicht, M., Van Cutsem, P., McCurdy, D.W., and Menzel, D. (2005). Cell wall pectins and xyloglucans are internalized into dividing root cells and accumulate within cell plates during cytokinesis. *Protoplasma* **225**: 141–155.
- Bechtold, N., Ellis, J., and Pelletier, G. (1993). In planta *Agrobacterium*-mediated gene transfer by infiltration of adult *Arabidopsis thaliana* plants. *Comp. Rend. L'Acad. des Sci. Serie III* **316**: 1194–1199.
- Beers, E.P. (1997). Programmed cell death during plant growth and development. *Cell Death Differ.* **4**: 649–661.
- Benková, E., Michniewicz, M., Sauer, M., Teichmann, T., Seifertová, D., Jürgens, G., and Friml, J. (2003). Local, efflux-dependent auxin gradients as a common module for plant organ formation. *Cell* **115**: 591–602.
- Bernasconi, P., Patel, B.C., Reagan, J.D., and Subramanian, M.V. (1996). The N-1-naphthylphthalamic acid-binding protein is an integral membrane protein. *Plant Physiol.* **111**: 427–432.
- Betz, W.J., Mao, F., and Smith, C.B. (1996). Imaging exocytosis and endocytosis. *Curr. Opin. Neurobiol.* **6**: 365–371.
- Blakeslee, J.J., et al. (2007). Interactions among PIN-FORMED and P-glycoprotein auxin transporters in *Arabidopsis*. *Plant Cell* **19**: 131–147.
- Boonsirichai, K., Sedbrook, J.C., Chen, R., Gilroy, S., and Masson, P.H. (2003). ALTERED RESPONSE TO GRAVITY is a peripheral membrane protein that modulates gravity-induced cytoplasmic

- alkalinization and lateral auxin transport in plant statocytes. *Plant Cell* **15**: 2612–2625.
- Bouchard, R., Bailly, A., Blakeslee, J.J., Oehring, S.C., Vincenzetti, V., Lee, O.R., Paponov, I., Palme, K., Mancuso, S., Murphy, A.S., Schulz, B., and Geisler, M.** (2006). Immunophilin-like TWISTED DWARF1 modulates auxin efflux activities of Arabidopsis P-glycoproteins. *J. Biol. Chem.* **281**: 30603–30612.
- Braccia, A., Villani, M., Immerdal, L., Niels-Christiansen, L.L., Nyström, B.T., Hansen, G.H., and Danielsen, E.M.** (2003). Microvillar membrane microdomains exist at physiological temperature. Role of galectin-4 as lipid raft stabilizer revealed by “superrafts”. *J. Biol. Chem.* **278**: 15679–15684.
- Brooks, D.R., Hooper, N.M., and Isaac, R.E.** (2003). The *Caenorhabditis elegans* orthologue of mammalian puromycin-sensitive aminopeptidase has roles in embryogenesis and reproduction. *J. Biol. Chem.* **278**: 42795–42801.
- Busse, J.S., and Evert, R.F.** (1999a). Pattern of differentiation of the first vascular elements in the embryo and seedling of *Arabidopsis thaliana*. *Int. J. Plant Sci.* **160**: 1–13.
- Busse, J.S., and Evert, R.F.** (1999b). Vascular differentiation and transition in the seedling of *Arabidopsis thaliana* (Brassicaceae). *Int. J. Plant Sci.* **160**: 241–251.
- Butler, J.H., Hu, S., Brady, S.R., Dixon, M.W., and Muday, G.K.** (1998). In vitro and in vivo evidence for actin association of the naphthylphthalamic acid-binding protein from zucchini hypocotyls. *Plant J.* **13**: 291–301.
- Chen, R., Hilson, P., Sedbrook, J., Rosen, E., Caspar, T., and Masson, P.H.** (1998). The *Arabidopsis thaliana* AGRVITROPIC 1 gene encodes a component of the polar-auxin-transport efflux carrier. *Proc. Natl. Acad. Sci. USA* **95**: 15112–15117.
- Chow, C.M., Neto, H., Foucart, C., and Moore, I.** (2008). Rab-A2 and Rab-A3 GTPases Define a *trans*-Golgi endosomal membrane domain in *Arabidopsis* that contributes substantially to the cell plate. *Plant Cell* **20**: 101–123.
- Clough, S.J., and Bent, A.F.** (1998). Floral dip: A simplified method for *Agrobacterium*-mediated transformation of *Arabidopsis thaliana*. *Plant J.* **16**: 735–743.
- Colón-Carmona, A., You, R., Haimovitch-Gal, T., and Doerner, P.** (1999). Technical advance: spatio-temporal analysis of mitotic activity with a labile cyclin-GUS fusion protein. *Plant J.* **20**: 503–508.
- Constam, D.B., Tobler, A.R., Rensing-Ehl, A., Kemler, I., Hersh, L.B., and Fontana, A.** (1995). Puromycin-sensitive aminopeptidase. Sequence analysis, expression, and functional characterization. *J. Biol. Chem.* **270**: 26931–26939.
- Cox, D.N., and Muday, G.K.** (1994). NPA binding activity is peripheral to the plasma membrane and is associated with the cytoskeleton. *Plant Cell* **6**: 1941–1953.
- Craft, J., Samalova, M., Baroux, C., Townley, H., Martinez, A., Jepson, I., Tsiantis, M., and Moore, I.** (2005). New pOP/LhG4 vectors for stringent glucocorticoid-dependent transgene expression in *Arabidopsis*. *Plant J.* **41**: 899–918.
- Cui, H., and Benfey, P.N.** (2009). Interplay between SCARECROW, GA and Like Heterochromatin Protein 1 in ground tissue patterning in the *Arabidopsis* root. *Plant J.* **2009**: 18.
- Cui, H., Levesque, M.P., Vernoux, T., Jung, J.W., Paquette, A.J., Gallagher, K.L., Wang, J.Y., Bliou, I., Scheres, B., and Benfey, P.N.** (2007). An evolutionarily conserved mechanism delimiting SHR movement defines a single layer of endodermis in plants. *Science* **316**: 421–425.
- de Gandarias, J.M., Irazusta, J., Gil, J., Gallego, M., Casis, O., and Casis, L.** (1997). Subcellular analysis of Tyr-aminopeptidase activities in the developing rat cerebellum. *Brain Res. Dev. Brain Res.* **99**: 66–71.
- Dhonukshe, P., Aniento, F., Hwang, I., Robinson, D.G., Mravec, J., Stierhof, Y.D., and Friml, J.** (2007). Clathrin-mediated constitutive endocytosis of PIN auxin efflux carriers in *Arabidopsis*. *Curr. Biol.* **17**: 520–527.
- Dhonukshe, P., Mathur, J., Hülskamp, M., and Gadella, T.W., Jr.** (2005). Microtubule plus-ends reveal essential links between intracellular polarization and localized modulation of endocytosis during division-plane establishment in plant cells. *BMC Biol.* **14**: 11–26.
- Fernando, R.N., Luff, S.E., Albiston, A.L., and Chai, S.Y.** (2007). Subcellular localization of insulin-regulated membrane aminopeptidase, IRAP to vesicles in neurons. *J. Neurochem.* **102**: 967–976.
- Friml, J.** (2003). Auxin transport - Shaping the plant. *Curr. Opin. Plant Biol.* **6**: 7–12.
- Friml, J., Vieten, A., Sauer, M., Weijers, D., Schwarz, H., Hamann, T., Offringa, R., and Jürgens, G.** (2003). Efflux-dependent auxin gradients establish the apical-basal axis of *Arabidopsis*. *Nature* **426**: 147–153.
- Galinha, C., Hofhuis, H., Luijten, M., Willemsen, V., Bliou, I., Heidstra, R., and Scheres, B.** (2007). PLETHORA proteins as dose-dependent master regulators of *Arabidopsis* root development. *Nature* **449**: 1053–1057.
- Gälweiler, L., Guan, C., Müller, A., Wisman, E., Mendgen, K., Yephremov, A., and Palme, K.** (1998). Regulation of polar auxin transport by AtPIN1 in *Arabidopsis* vascular tissue. *Science* **282**: 2226–2230.
- Garbers, C., DeLong, A., Deruére, J., Bernasconi, P., and Söll, D.** (1996). A mutation in protein phosphatase 2A regulatory subunit A affects auxin transport in *Arabidopsis*. *EMBO J.* **15**: 2115–2124.
- Geisler, M., et al.** (2005). Cellular efflux of auxin catalyzed by the *Arabidopsis* MDR/PGP transporter AtPGP1. *Plant J.* **44**: 179–194.
- Geisler, M., et al.** (2003). TWISTED DWARF1, a unique plasma membrane-anchored immunophilin-like protein, interacts with *Arabidopsis* multidrug resistance-like transporters AtPGP1 and AtPGP19. *Mol. Biol. Cell* **14**: 4238–4249.
- Geldner, N., Anders, N., Wolters, H., Keicher, J., Kornberger, W., Müller, P., Delbarre, A., Ueda, T., Nakano, A., and Jürgens, G.** (2003). The *Arabidopsis* GNOM ARF-GEF mediates endosomal recycling, auxin transport, and auxin-dependent plant growth. *Cell* **112**: 219–230.
- Geldner, N., Friml, J., Stierhof, Y.D., Jürgens, G., and Palme, K.** (2001). Auxin transport inhibitors block PIN1 cycling and vesicle trafficking. *Nature* **413**: 425–428.
- Geldner, N., Richter, S., Vieten, A., Marquardt, S., Torres-Ruiz, R.A., Mayer, U., and Jürgens, G.** (2004). Partial loss-of-function alleles reveal a role for GNOM in auxin transport-related, post-embryonic development of *Arabidopsis*. *Development* **131**: 389–400.
- Gil, P., Dewey, E., Friml, J., Zhao, Y., Snowden, K.C., Putterill, J., Palme, K., Estelle, M., and Chory, J.** (2001). BIG: a calossin-like protein required for polar auxin transport in *Arabidopsis*. *Genes Dev.* **15**: 1985–1997.
- Goujon, T., Minic, Z., El Amrani, A., Lerouxel, O., Aletti, E., Lapierre, C., Joseleau, J.P., and Jouanin, L.** (2003). AtBXL1, a novel higher plant (*Arabidopsis thaliana*) putative beta-xylosidase gene, is involved in secondary cell wall metabolism and plant development. *Plant J.* **33**: 677–690.
- Gray, W.M., Muskett, P.R., Chuang, H.W., and Parker, J.E.** (2003). *Arabidopsis* SGT1b is required for SCF(TIR1)-mediated auxin response. *Plant Cell* **15**: 1310–1319.
- Griffith, M.E., Mayer, U., Capron, A., Ngo, Q.A., Surendrarao, A., McClinton, R., Jürgens, G., and Sundaresan, V.** (2007). The TORMOZ gene encodes a nucleolar protein required for regulated division planes and embryo development in *Arabidopsis*. *Plant Cell* **19**: 2246–2263.

- Guillon, F., Philippe, S., Bouchet, B., Devaux, M.F., Frasse, P., Jones, B., Bouzayen, M., and Lahaye, M. (2008). Down-regulation of an Auxin Response Factor in the tomato induces modification of fine pectin structure and tissue architecture. *J. Exp. Bot.* **59**: 273–288.
- Guimil, S., and Dunand, C. (2007). Cell growth and differentiation in *Arabidopsis* epidermal cells. *J. Exp. Bot.* **58**: 3829–3840.
- Hakman, I., Hallberg, H., and Palovaara, J. (2009). The polar auxin transport inhibitor NPA impairs embryo morphology and increases the expression of an auxin efflux facilitator protein PIN during *Picea abies* somatic embryo development. *Tree Physiol.* **29**: 483–496.
- Hardtke, C.S., and Berleth, T. (1998). The *Arabidopsis* gene MONOPTEROS encodes a transcription factor mediating embryo axis formation and vascular development. *EMBO J.* **17**: 1405–1411.
- Hamann, T., Benkova, E., Bäurle, I., Kientz, M., and Jürgens, G. (2002). The *Arabidopsis* BODENLOS gene encodes an auxin response protein inhibiting MONOPTEROS-mediated embryo patterning. *Genes Dev.* **16**: 1610–1615.
- Hamann, T., Mayer, U., and Jurgens, G. (1999). The auxin-insensitive bodenlos mutation affects primary root formation and apical-basal patterning in the *Arabidopsis* embryo. *Development* **126**: 1387–1395.
- Hattori, A., Kitatani, K., Matsumoto, H., Miyazawa, S., Rogi, T., Tsuruoka, N., Mizutani, S., Natori, Y., and Tsujimoto, M. (2000). Characterization of recombinant human adipocyte-derived leucine aminopeptidase expressed in Chinese hamster ovary cells. *J. Biochem.* **128**: 755–757.
- Herbst, A., Wolner-Hanssen, P., and Ingemarsson, I. (1997). Risk factors for acidemia at birth. *Obstet. Gynecol.* **90**: 125–130.
- Hesp, J.R., and Hooper, N.M. (1997). Proteolytic fragmentation reveals the oligomeric and domain structure of porcine aminopeptidase A. *Biochemistry* **36**: 3000–3007.
- Illinger, D., and Kuhry, J.G. (1994). The kinetic aspects of intracellular fluorescence labeling with TMA-DPH support the maturation model for endocytosis in L929 cells. *J. Cell Biol.* **125**: 783–794.
- Jaillais, Y., Fobis-Loisy, I., Miège, C., Rollin, C., and Gaude, T. (2006). AtSNX1 defines an endosome for auxin-carrier trafficking in *Arabidopsis*. *Nature* **443**: 106–109.
- Jones, B., Frasse, P., Olmos, E., Zegzouti, H., Li, Z.G., Latché, A., Pech, J.C., and Bouzayen, M. (2002). Down-regulation of DR12, an auxin-response-factor homolog, in the tomato results in a pleiotropic phenotype including dark green and blotchy ripening fruit. *Plant J.* **32**: 603–613.
- Jürgens, G. (2001). Apical-basal pattern formation in *Arabidopsis* embryogenesis. *EMBO J.* **20**: 3609–3616.
- Kleine-Vehn, J., Dhonukshe, P., Swarup, R., Bennett, M., and Friml, J. (2006). Subcellular trafficking of the *Arabidopsis* auxin influx carrier AUX1 uses a novel pathway distinct from PIN1. *Plant Cell* **18**: 3171–3181.
- Kramer, W., Girbig, F., Corsiero, D., Pfenninger, A., Frick, W., Jahne, G., Rhein, M., Wendler, W., Lottspeich, F., Hochleitner, E.O., Orso, E., and Schmitz, G. (2005). Aminopeptidase N (CD13) is a molecular target of the cholesterol absorption inhibitor ezetimibe in the enterocyte brush border membrane. *J. Biol. Chem.* **280**: 1306–1320.
- Kunst, L., Browse, J., and Somerville, C. (1988). Altered regulation of lipid biosynthesis in a mutant of *Arabidopsis* deficient in chloroplast glycerol-3-phosphate acyltransferase activity. *Proc. Natl. Acad. Sci. USA* **85**: 4143–4147.
- Larsson, E., Sitbon, F., Ljung, K., and von Arnold, S. (2008). Inhibited polar auxin transport results in aberrant embryo development in Norway spruce. *New Phytol.* **177**: 356–366.
- Lefevre, P., Witham, J., Lacroix, C.E., Cockerill, P.N., Bonifer, C. (2008). The LPS-induced transcriptional upregulation of the chicken lysozyme locus involves CTCF eviction and noncoding RNA transcription. *Mol Cell.* **232**: 129–139.
- Lewis, D.R., Miller, N.D., Splitt, B.L., Wu, G., and Spalding, E.P. (2007). Separating the roles of acropetal and basipetal auxin transport on gravitropism with mutations in two *Arabidopsis* multidrug resistance-like ABC transporter genes. *Plant Cell* **19**: 1838–1850.
- Li, J., et al. (2005). *Arabidopsis* H⁺-PPase AVP1 regulates auxin-mediated organ development. *Science* **310**: 121–125.
- Lim, S.N., Bonzelius, F., Low, S.H., Wille, H., Weimbs, T., and Herman, G.A. (2001). Identification of discrete classes of endosome-derived small vesicles as a major cellular pool for recycling membrane proteins. *Mol. Biol. Cell* **12**: 981–995.
- Luan, Y., and Xu, W. (2007). The structure and main functions of aminopeptidase N. *Curr. Med. Chem.* **14**: 639–647.
- Luschnig, C., Gaxiola, R.A., Grisafi, P., and Fink, G.R. (1998). EIR1, a root-specific protein involved in auxin transport, is required for gravitropism in *Arabidopsis thaliana*. *Genes Dev.* **12**: 2175–2187.
- Lyczak, R., Zweier, L., Group, T., Murrow, M.A., Snyder, C., Kulovitz, L., Beatty, A., Smith, K., and Bowerman, B. (2006). The puromycin-sensitive aminopeptidase PAM-1 is required for meiotic exit and anteroposterior polarity in the one-cell *Caenorhabditis elegans* embryo. *Development* **133**: 4281–4292.
- Macquet, A., Ralet, M.C., Loudet, O., Kronenberger, J., Mouille, G., Marion-Poll, A., and North, H.M. (2007). A naturally occurring mutation in an *Arabidopsis* accession affects a beta-D-galactosidase that increases the hydrophilic potential of rhamnogalacturonan I in seed mucilage. *Plant Cell* **19**: 3990–4006.
- Makam, S.N., Peer, W.A., Blakeslee, J.J., and Murphy, A.S. (2005). Cultural conditions contributing to vine decline syndrome in watermelon. *HortScience* **40**: 597–601.
- Marchant, A., Kargul, J., May, S.T., Muller, P., Delbarre, A., Perrot-Rechenmann, C., and Bennett, M.J. (1999). AUX1 regulates root gravitropism in *Arabidopsis* by facilitating auxin uptake within root apical tissues. *EMBO J.* **18**: 2066–2073.
- Mayer, U., Buttner, G., and Jurgens, G. (1993). Apical-basal pattern formation in the *Arabidopsis* embryo - studies on the role of the GNOM gene. *Development* **117**: 149–162.
- Mayer, U., Torres Ruiz, R.A., Berleth, T., Miséra, S., and Jürgens, G. (1991). Mutations affecting body organization in the *Arabidopsis* embryo. *Nature* **353**: 402–407.
- McCann, M.C., Wells, B., and Roberts, K. (1992). Complexity in the spatial localization and length distribution of plant cell-wall matrix polysaccharides. *J. Microsc.* **166**: 123–136.
- Men, S., Boutté, Y., Ikeda, Y., Li, X., Palme, K., Stierhof, Y.D., Hartmann, M.A., Moritz, T., and Grebe, M. (2008). Sterol-dependent endocytosis mediates post-cytokinetic acquisition of PIN2 auxin efflux carrier polarity. *Nat. Cell Biol.* **10**: 237–244.
- Mongrand, S., Morel, J., Laroche, J., Claverol, S., Carde, J.P., Hartmann, M.A., Bonneau, M., Simon-Plas, F., Lessire, R., and Bessoule, J.J. (2004). Lipid rafts in higher plant cells: Purification and characterization of Triton X-100-insoluble microdomains from tobacco plasma membrane. *J. Biol. Chem.* **279**: 36277–36286.
- Moore, I., Samalova, M., and Kurup, S. (2006). Transactivated and chemically inducible gene expression in plants. *Plant J.* **45**: 651–683.
- Mravec, J., Kubes, M., Bielach, A., Gaykova, V., Petrásek, J., Skúpa, P., Chand, S., Benková, E., Zazimalová, E., and Friml, J. (2008). Interaction of PIN and PGP transport mechanisms in auxin distribution-dependent development. *Development* **135**: 3345–3354.
- Müller, A., Guan, C., Gälweiler, L., Tänzler, P., Huijser, P., Marchant, A., Parry, G., Bennett, M., Wisman, E., and Palme, K. (1998). AtPIN2 defines a locus of *Arabidopsis* for root gravitropism control. *EMBO J.* **17**: 6903–6911.
- Murphy, A., and Taiz, L. (1999a). Localization and characterization of soluble and plasma membrane aminopeptidase activities in *Arabidopsis* seedlings. *Plant Physiol. Biochem.* **37**: 431–443.

- Murphy, A., and Taiz, L.** (1999b). Naphthylphthalamic acid is enzymatically hydrolyzed at the hypocotyl-root transition zone and other tissues of *Arabidopsis thaliana* seedlings. *Plant Physiol. Biochem.* **37**: 413–430.
- Murphy, A., Peer, W.A., and Taiz, L.** (2000). Regulation of auxin transport by aminopeptidases and endogenous flavonoids. *Planta* **211**: 315–324.
- Murphy, A.S., Hoogner, K.R., Peer, W.A., and Taiz, L.** (2002). Identification, purification, and molecular cloning of N-1-naphthylphthalamic acid-binding plasma membrane-associated aminopeptidases from *Arabidopsis*. *Plant Physiol.* **128**: 935–950.
- Nebenführ, A., Ritzenthaler, C., and Robinson, D.G.** (2002). Brefeldin A: Deciphering an enigmatic inhibitor of secretion. *Plant Physiol.* **130**: 1102–1108.
- Noh, B., Bandyopadhyay, A., Peer, W.A., Spalding, E.P., and Murphy, A.S.** (2003). Enhanced gravi- and phototropism in plant *mdr* mutants mislocalizing the auxin efflux protein PIN1. *Nature* **423**: 999–1002.
- Noh, B., Murphy, A.S., and Spalding, E.P.** (2001). Multidrug resistance-like genes of *Arabidopsis* required for auxin transport and auxin-mediated development. *Plant Cell* **13**: 2441–2454.
- Ofer, L.D., and Hooper, N.M.** (2002). The C-terminal domain, but not the interchain disulphide, is required for the activity and intracellular trafficking of aminopeptidase A. *Biochem. J.* **362**: 191–197.
- Okada, K., Ueda, J., Komaki, M.K., Bell, C.J., and Shimura, Y.** (1991). Requirement of the auxin polar transport system in early stages of *Arabidopsis* floral bud formation. *Plant Cell* **3**: 677–684.
- Osada, T., Watanabe, G., Kondo, S., Toyoda, M., Sakaki, Y., and Takeuchi, T.** (2001b). Male reproductive defects caused by puromycin-sensitive aminopeptidase deficiency in mice. *Mol. Endocrinol.* **15**: 960–971.
- Osada, T., Watanabe, G., Sakaki, Y., and Takeuchi, T.** (2001a). Puromycin-sensitive aminopeptidase is essential for the maternal recognition of pregnancy in mice. *Mol. Endocrinol.* **15**: 882–893.
- Otegui, M.S., Capp, R., and Staehelin, L.A.** (2002). Developing seeds of *Arabidopsis* store different minerals in two types of vacuoles and in the endoplasmic reticulum. *Plant Cell* **14**: 1–17.
- Paciorek, T., Zazimalová, E., Ruthardt, N., Petrásek, J., Stierhof, Y. D., Kleine-Vehn, J., Morris, D.A., Emans, N., Jürgens, G., Geldner, N., and Friml, J.** (2005). Auxin inhibits endocytosis and promotes its own efflux from cells. *Nature* **435**: 1251–1256.
- Pan, J., Fujioka, S., Peng, J., Chen, J., Li, G., and Chen, R.** (2009). The E3 ubiquitin ligase SCF^{TIR1/AFB} and membrane sterols play key roles in auxin regulation of endocytosis, recycling, and plasma membrane accumulation of the auxin efflux transporter PIN2 in *Arabidopsis thaliana*. *Plant Cell* **21**: 568–580.
- Papadopoulos, T., Heuer, H., and Bauer, K.** (2000). Analysis of the thyrotropin-releasing hormone-degrading ectoenzyme by site-directed mutagenesis of cysteine residues. Cys68 is involved in disulfide-linked dimerization. *Eur. J. Biochem.* **267**: 2617–2623.
- Peer, W.A., Bandyopadhyay, A., Blakeslee, J.J., Makam, S.N., Chen, R., Mason, P., and Murphy, A.** (2004). Variation in expression and protein localization of the PIN family of auxin efflux facilitator proteins in flavonoid mutants with altered auxin transport in *Arabidopsis thaliana*. *Plant Cell* **16**: 1898–1911.
- Peer, W.A., and Murphy, A.S.** (2007). Flavonoids and auxin transport: Modulators or regulators? *Trends Plant Sci.* **12**: 556–563.
- Petrásek, J., Cerná, A., Schwarzerová, K., Eickner, M., Morris, D.A., and Zazimalová, E.** (2003). Do phototropins inhibit auxin efflux by impairing vesicle traffic? *Plant Physiol.* **131**: 254–263.
- Pradillo, M., López, E., Romero, C., Sánchez-Morán, E., Cuñado, N., and Santos, J.L.** (2007). An analysis of univalent segregation in meiotic mutants of *Arabidopsis thaliana*: A possible role for synaptonemal complex. *Genetics* **175**: 505–511.
- Reape, T.J., and McCabe, P.F.** (2008). Apoptotic-like programmed cell death in plants. *New Phytol.* **180**: 13–26.
- Robert, S., Chary, S.N., Drakakaki, G., Li, S., Yang, Z., Raikhel, N.V., and Hicks, G.R.** (2008). Endosidin1 defines a compartment involved in endocytosis of the brassinosteroid receptor BRI1 and the auxin transporters PIN2 and AUX1. *Proc. Natl. Acad. Sci. USA* **105**: 8464–8469.
- Robinson, D.G., Jiang, L., and Schumacher, K.** (2008b). The endosomal system of plants: Charting new and familiar territories. *Plant Physiol.* **147**: 1482–1492.
- Robinson, D.G., Langhans, M., Saint-Jore-Dupas, C., and Hawes, C.** (2008a). BFA effects are tissue and not just plant specific. *Trends Plant Sci.* **13**: 405–408.
- Rojas-Pierce, M., Titapiwatanakun, B., Sohn, E.J., Fang, F., Larive, C.K., Blakeslee, J., Cheng, Y., Cutler, S.R., Peer, W.A., Murphy, A.S., and Raikhel, N.V.** (2007). *Arabidopsis* P-glycoprotein19 participates in the inhibition of gravitropism by gravacin. *Chem. Biol.* **14**: 1366–1376.
- Rozenfeld, R., Muller, L., El Messari, S., and Llorens-Cortes, C.** (2004). The C-terminal domain of aminopeptidase A is an intramolecular chaperone required for the correct folding, cell surface expression, and activity of this monozinc aminopeptidase. *J. Biol. Chem.* **279**: 43285–43295.
- Růžicka, K., Ljung, K., Vanneste, S., Podhorská, R., Beeckman, T., Friml, J., and Benková, E.** (2007). Ethylene regulates root growth through effects on auxin biosynthesis and transport-dependent auxin distribution. *Plant Cell* **19**: 2197–2212.
- Sabatini, S., Heidstra, R., Wildwater, M., and Scheres, B.** (2003). SCARECROW is involved in positioning the stem cell niche in the *Arabidopsis* root meristem. *Genes Dev.* **17**: 354–358.
- Saint-Jore, C.M., Evins, J., Batoko, H., Brandizzi, F., Moore, I., and Hawes, C.** (2002). Redistribution of membrane proteins between the Golgi apparatus and endoplasmic reticulum in plants is reversible and not dependent on cytoskeletal networks. *Plant J.* **29**: 661–678.
- Sanchez-Moran, E., Jones, G., Franklin, F., and Santos, J.** (2004). A puromycin-sensitive aminopeptidase is essential for meiosis in *Arabidopsis thaliana*. *Plant Cell* **16**: 2895–2909.
- Schnittger, A., Schöbinger, U., Stierhof, Y., and Hülskamp, M.** (2002). Ectopic B-type cyclin expression induces mitotic cycles in endoreplicating *Arabidopsis* trichomes. *Curr. Biol.* **12**: 415–420.
- Shevell, D.E., Kunkel, T., and Chua, N.H.** (2000). Cell wall alterations in the *Arabidopsis emb30* mutant. *Plant Cell* **12**: 2047–2060.
- Shin, H., Shin, H.S., Guo, Z., Blancaflor, E.B., Masson, P.H., and Chen, R.** (2005). Complex regulation of *Arabidopsis* AGR1/PIN2-mediated root gravitropic response and basipetal auxin transport by cantharidin-sensitive protein phosphatases. *Plant J.* **42**: 188–200.
- Smith, A.P., Nourizadeh, S.D., Peer, W.A., Xu, J., Bandyopadhyay, A., Murphy, A.S., and Goldsbrough, P.B.** (2003). *Arabidopsis* AtGSTF2 is regulated by ethylene and auxin, and encodes a glutathione S-transferase that interacts with flavonoids. *Plant J.* **36**: 433–442.
- Steinmann, T., Geldner, N., Grebe, M., Mangold, S., Jackson, C.L., Paris, S., Gälweiler, L., Palme, K., Jürgens, G.** (1999). Coordinated polar localization of auxin efflux carrier PIN1 by GNOM ARF GEF. *Science* **286**: 316–318.
- Stieger, P.A., Reinhardt, D., and Kuhlemeier, C.** (2002). The auxin influx carrier is essential for correct leaf positioning. *Plant J.* **32**: 509–517.
- Swarup, R., Friml, J., Marchant, A., Ljung, K., Sandberg, G., Palme, K., and Bennett, M.** (2001). Localization of the auxin permease AUX1 suggests two functionally distinct hormone transport pathways operate in the *Arabidopsis* root apex. *Genes Dev.* **15**: 2648–2653.
- ten Hove, C.A., and Heidstra, R.** (2008). Who begets whom? Plant cell

- fate determination by asymmetric cell division. *Curr. Opin. Plant Biol.* **11**: 34–41.
- Terasaka, K., Blakeslee, J.J., Titapiwatanakun, B., Peer, W.A., Bandyopadhyay, A., Makam, S.N., Lee, O.R., Richards, E.L., Murphy, A.S., Sato, F., and Yazaki, K.** (2005). PGP4, an ATP binding cassette P-glycoprotein, catalyzes auxin transport in *Arabidopsis thaliana* roots. *Plant Cell* **17**: 2922–2939.
- Till, B.J., et al.** (2003). Large-scale discovery of induced point mutations with high-throughput TILLING. *Genome Res.* **13**: 524–530.
- Titapiwatanakun, B., et al.** (2009). ABCB19/PGP19 stabilises PIN1 in membrane microdomains in *Arabidopsis*. *Plant J.* **57**: 27–44.
- Towne, C.F., York, I.A., Neijssen, J., Karow, M.L., Murphy, A.J., Valenzuela, D.M., Yancopoulos, G.D., Neefjes, J.J., and Rock, K.L.** (2008). Puromycin-sensitive aminopeptidase limits MHC class I presentation in dendritic cells but does not affect CD8 T cell responses during viral infections. *J. Immunol.* **180**: 1704–1712.
- Truernit, E., Bauby, H., Dubreucq, B., Grandjean, O., Runions, J., Barthélémy, J., and Palauqui, J.C.** (2008). High-resolution whole-mount imaging of three-dimensional tissue organization and gene expression enables the study of Phloem development and structure in *Arabidopsis*. *Plant Cell* **20**: 1494–1503.
- Tse, Y.C., Lo, S.W., Hillmer, S., Dupree, P., and Jiang, L.** (2006). Dynamic response of prevacuolar compartments to brefeldin A in plant cells. *Plant Physiol.* **142**: 1442–1459.
- Tsujimoto, M., Mizutani, S., Adachi, H., Kimura, M., Nakazato, H., and Tomoda, Y.** (1992). Identification of human placental leucine aminopeptidase as oxytocinase. *Arch. Biochem. Biophys.* **292**: 388–392.
- Ueda, T., Uemura, T., Sato, M.H., and Nakano, A.** (2004). Functional differentiation of endosomes in *Arabidopsis* cells. *Plant J.* **40**: 783–789.
- Ueda, T., Yamaguchi, M., Uchimiya, H., and Nakano, A.** (2001). Ara6, a plant-unique novel type Rab GTPase, functions in the endocytic pathway of *Arabidopsis thaliana*. *EMBO J.* **20**: 4730–4741.
- Ulmasov, T., Murfett, J., Hagen, G., and Guilfoyle, T.J.** (1997). Aux/IAA proteins repress expression of reporter genes containing natural and highly active synthetic auxin response elements. *Plant Cell* **9**: 1963–1971.
- Weijers, D., Sauer, M., Meurette, O., Friml, J., Ljung, K., Sandberg, G., Hooykaas, P., and Offringa, R.** (2005). Maintenance of embryonic auxin distribution for apical-basal patterning by PIN-FORMED-dependent auxin transport in *Arabidopsis*. *Plant Cell* **17**: 2517–2526.
- Welch, D., Hassan, H., Bliilou, I., Immink, R., Heidstra, R., and Scheres, B.** (2007). *Arabidopsis* JACKDAW and MAGPIE zinc finger proteins delimit asymmetric cell division and stabilize tissue boundaries by restricting SHORT-ROOT action. *Genes Dev.* **21**: 2196–2204.
- Western, T.L., Skinner, D.J., and Haughn, G.W.** (2000). Differentiation of mucilage secretory cells of the *Arabidopsis* seed coat. *Plant Physiol.* **122**: 345–355.
- Wisniewska, J., Xu, J., Seifertová, D., Brewer, P.B., Ruzicka, K., Bliilou, I., Rouquié, D., Benková, E., Scheres, B., and Friml, J.** (2006). Polar PIN localization directs auxin flow in plants. *Science* **312**: 883.
- Wulfaenger, J., Niedling, S., Riemann, D., and Seliger, B.** (2008). Aminopeptidase N (APN)/CD13-dependent CXCR4 downregulation is associated with diminished cell migration, proliferation and invasion. *Mol. Membr. Biol.* **25**: 72–82.
- Wysocka-Diller, J.W., Helariutta, Y., Fukaki, H., Malamy, J.E., and Benfey, P.N.** (2000). Molecular analysis of SCARECROW function reveals a radial patterning mechanism common to root and shoot. *Development* **127**: 595–603.